Volume 5 OCTOBER, 1934 Number 10

PHYSICS

A Journal of General and Applied Physics

Some New Sedimentation Formulas

HAKON WADELL, *University of Chicago*

(Received April 6, 1934)

This paper presents some new methods of computing the sedimentation radius. The methods are founded on a curve for spheres, experimentally determined and constructed on the basis of the coefficient of resistance as a function of Reynolds number. When the validity of Stokes' law ceases, the sedimentation radius obtained by Stokes' formula is graphically corrected. The amount of deviation of Stokes' law from experimental data of higher Reynolds numbers has been statistically determined. Some new formulas for computing the resistance and the radius of a sphere of a given terminal settling velocity are presented.

SOME NEW TERMS AND NOTATIONS

SCHÖNE[1] introduced in 1868 the term *hydraulic value* (hydraulischer Werth), meaning thereby the diameter size of a quartz sphere having the same settling velocity as a given particle in water as sedimentation medium. Thus the hydraulic value has no bearing on the actual size of the particle. An improvement was made by Odén[2] in 1915 by introducing the conception *equivalent radius*, i.e., the radius of a sphere of the same material and of the same settling velocity as a given particle. The sedimentation medium is not expressively stated, but one infers from Odén's writing that water is used as sedimentation fluid. Although I believe that Odén by "the same material" means the *same specific gravity*, the definition is not sharp. The specific gravity value, but not the material, enters the sedimentation formula. The term *equivalent radius* as synonymous with the radius of a sphere of equivalent settling velocity is slightly confusing, if one wishes to use the expressions *equivalent volume*, *equivalent surface*, etc. In conclusion, I believe that a new term *sedimentation radius* is justified. Definition: *The sedimentation radius is the radius of a sphere of the same specific gravity and of the same terminal uniform settling velocity as a given particle in the same sedimentation fluid.* The term does not imply any special kind of sedimentation medium, and the kind of fluid used must be stated in each case. The values obtained for the sedimentation radius in different fluids are not comparable above Reynolds number 0.2, except when the particles are perfect spheres.

The diameter and the radius of a sphere of the same volume as a given, spherical or non-spherical, solid have been previously introduced as the *true nominal diameter* and the *true nominal radius*, respectively.[3, 4, 5]

[1] Em. Schöne, *Ueber einen neuen Apparat für die Schlämmanalyse*, Zeits. f. analyt. Chemie **7**, 29 (1868).

[2] S. Odén, *Eine neue Methode zur mechanischen Bodenanalyse*, Int. Mitt. f. Bodenkunde **5**, 257 (1915).

[3] H. Wadell, *Volume, Shape and Roundness of Rock Particles*, J. Geology **40**, 443 (1932).

[4] H. Wadell, *Sphericity and Roundness of Rock Particles*, J. Geology **41**, 310 (1933).

[5] H. Wadell, *The Coefficient of Resistance as a Function of Reynolds Number for Solids of Various Shapes*, J. Frank. Inst. **217**, 459 (1934).

The *actual radius* is an emphasized expression for the radius of a perfect sphere. The term is used as a contrast to the *Stokes radius*, which is the radius of a perfect sphere computed according to Stokes' law. The Stokes radius is always smaller than the actual radius for Reynolds numbers higher than 0.2. The *Stokes sedimentation radius* signifies that the sedimentation radius has been computed according to Stokes' law. The *Stokes velocity* signifies the terminal uniform settling velocity computed according to Stokes' formula for spheres.

The conception *degree of true sphericity* has been previously introduced[3, 4, 5] as a sedimentological shape expression based on the isoperimetric property of a sphere and expressed by the formula: $\psi = s/S$, where ψ is the degree of true sphericity, s the surface area of a sphere of the same volume as the solid, and S the actual surface area of the solid. The maximum value obtained by this formula is 1.000, which is the degree of true sphericity of a sphere.

The *easiest shape position* is that position in which a solid of a given shape attains its maximum terminal uniform settling velocity. The *tardiest shape position* signifies the position of minimum velocity. The *average shape position* is understood to be a great number of positions in which the solid attains different velocities, the mean of which constitutes the *average velocity*. Except for spheres, all shapes have an easiest and a tardiest shape position.

The Coefficient of Resistance as a Function of Reynolds Number for Solids of Various Shapes

The force, acting upon a falling particle immersed in a fluid, equals the effective weight of the solid. When the particle has attained its terminal velocity this force (F) is exactly balanced by the fluid resistance, R:

$$F = R = Mg = (4/3)\pi r_n^3(\rho_S - \rho_F)g, \qquad (1)$$

where M is the mass, r_n the true nominal radius, ρ_S the specific gravity of the solid, ρ_F the specific gravity of the fluid, and g the acceleration of gravity. It follows that the resistance, R, must always be the same for solids of the same specific gravity, of the same true nominal radius (or the same volume) and immersed in the same fluid, irrespective of shape and shape position of the solids, *nota bene*, when the terminal velocities of respective solids have been attained. The terminal velocity, which also is the maximum velocity, varies with the shape and shape position and also with the Reynolds number. This variation is conveniently expressed by the so-called *coefficient of resistance*. A slight change, by inserting the true nominal radius in conventional formulas for the coefficient of resistance and the Reynolds number for spheres, has been previously suggested.[5] The formulas become thereby applicable to all shapes and shape positions, and the coefficient of resistance as a function of Reynolds number expresses the influence which the properties of the fluid and of the solid have on the terminal uniform settling velocity. The formulas read:

$$C_R = 8r_n(\rho_S - \rho_F)g/3v^2\rho_F, \qquad (2)$$

$$\mathbf{R} = 2r_n v\rho_F/\mu = 2r_n v/\nu, \qquad (3)$$

where C_R is the coefficient of resistance, r_n the true nominal radius, ρ_S the specific gravity of the solid, ρ_F the specific gravity of the fluid, μ the viscosity coefficient of the fluid, ν the kinematic viscosity μ/ρ_F, g the acceleration of gravity, and $\mathbf{R}$ Reynolds number.

The coefficient of resistance as a function of Reynolds number for spheres is shown in Figs. 1, 2, 3 and 4. The curve represents the results obtained by Allen,[6] Arnold,[7] Liebster,[8] Schmiedel,[9] Wieselsberger, Betz and Prandtl.[10] Ladenburg's[11] correction for the influence of the wall of the sedimentation vessel has been taken into consideration, whenever the corrected experimental data have been available. Schiller's[12] tables have

[6] H. S. Allen, *The Motion of a Sphere in a Viscous Fluid*, Phil. Mag. [5] **50**, 323, 519 (1900).

[7] H. D. Arnold, *Limitations Imposed by Slip and Inertia Terms upon Stokes' Law for the Motion of Spheres Through Liquids*, Phil. Mag. [6] **22**, 755 (1911).

[8] H. Liebster, *Über den Widerstand von Kugeln*, Ann. d. Physik [4] **82**, 541 (1927).

[9] J. Schmiedel, *Experimentelle Untersuchungen über die Fallbewegung von Kugeln und Scheiben in reibenden Flüssigkeiten*, Phys. Zeits. **29**, 593 (1928).

[10] C. Wieselsberger, A. Betz, L. Prandtl, *Ergebnisse der aerodynamischen Versuchsanstalt zu Göttingen*, Part II (1923).

[11] R. Ladenburg, *Über den Einfluss von Wänden auf die Bewegung einer Kugel in einer reibenden Flüssigkeit*, Ann. d. Physik [4] **23**, 447 (1907).

[12] L. Schiller, *Fallversuche mit Kugeln und Scheiben*, Handb. d. exp. Physik (Ed. by W. Wien and F. H. Harms), **4**, No. 2, *Hydro- und Aerodynamik*, pp. 337–387 (1932).

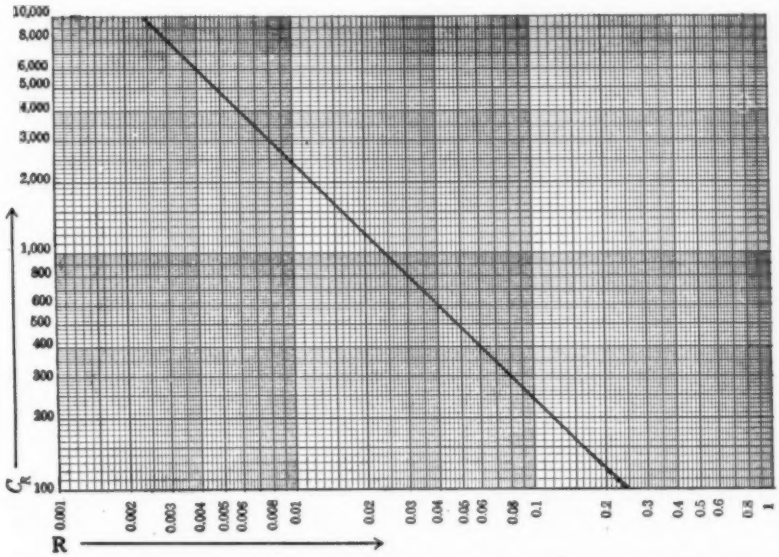

FIG. 1. Coefficient of resistance as a function of Reynolds number for spheres.

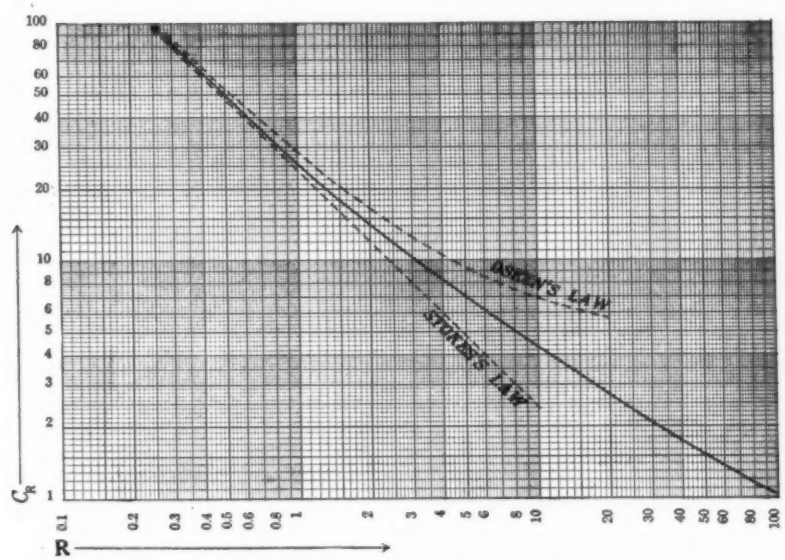

FIG. 2. Coefficient of resistance as a function of Reynolds number for spheres.

also been consulted. The dotted curves represent the coefficient of resistance as a function of Reynolds number $[C_R=f(\mathbf{R})]$ according to Stokes' and Oseen's formulas for spheres. Chart Fig. 5 illustrates the dispersion of the experimental data, expressed by the $C_R=f(\mathbf{R})$ according to results obtained by Allen,[6] Liebster,[8] Schmiedel,[9] Wieselsberger[10] and Lunnon.[13] All data are represented *without* Ladenburg's or Faxén's[14] corrections. Allen's results refer to his spheres of amber and of steel in water. The data for the single dot representing Lunnon's result have been taken from a table by Schiller.[12]

It has been shown in a previous paper[5] that the curves, constructed on the basis of the $C_R=f(\mathbf{R})$ for solids of various shapes (sphericity values), become asymptotic towards lower Reynolds numbers. Within the region of laminar

[13] R. G. Lunnon, *Fluid Resistance to Moving Spheres*, Proc. Roy. Soc. (London) **A118**, 680 (1928).

[14] H. Faxén, *Die Bewegung einer starren Kugel längs der Achse eines mit zäher Flüssigkeit gefüllten Rohres*, Arkiv f. Matematik, Astronomi och Fysik **17**, No. 27 (1923).

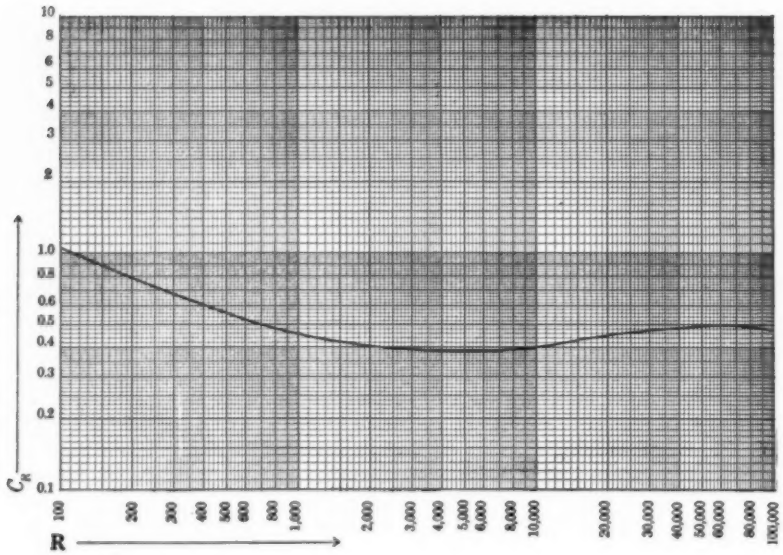

FIG. 3. Coefficient of resistance as a function of Reynolds number for spheres.

motion of the fluid about the solid, i.e., within the region of Stokes' law, the $C_R=f(\mathbf{R})$ for a given shape and shape position appears to take a linear trend parallel with the linear function of Stokes' law for spheres. On account of rotational motion of the fluid the effect of the shape increases with increasing Reynolds number, so that the distance between the curve for spheres and the $C_R=f(\mathbf{R})$ for a given shape and shape position increases with increasing **R**-value. As a consequence, the difference in size between the sedimentation radius, r_s, and that of the true nominal radius, r_n, increases with increasing Reynolds number for a given shape and shape position. An example is given in Table I. Solids Nos. 2, 3 and 4 have the same shape positions and almost the same shape ($\psi=0.2182$ to 0.2375). The Reynolds number increases from 0.1389 (solid No. 2) to 7881 (solid No. 4).[15, 16] Among the symbols in the table *th* represents the thickness of a disk, r_d the radius of the flat face of the disk, r_n the true nominal radius, r_{sSt} the Stokes' sedimentation radius, and r_s the sedimentation radius determined by methods described in a latter part of this paper. For the solids Nos. 2, 3 and 4 the ratios r_n/r_s and *volume of a sphere of radius* r_n*/volume of a sphere of radius* r_s are as follows:

Solid No.	$\frac{r_n}{r_s}$	$\frac{\text{Volume of sphere of radius } r_n}{\text{Volume of sphere of radius } r_s}$
2	1.6	4.6
3	2.4	16.0
4	12.3	1870.5

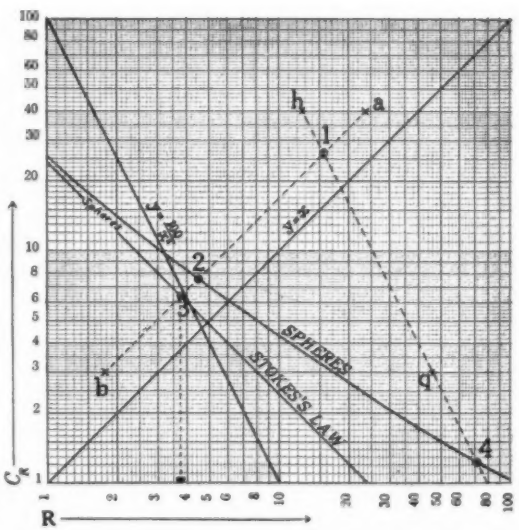

FIG. 4. Coefficient of resistance as a function of Reynolds number for spheres.

[15] V. Pernolet, *A l'étude des préparations mécaniques des minerais, ou expériences propres à établir la théorie des différent systèmes usités ou possibles*, Ann. des Mines [4] **20**, 390 (1851).

[16] H. Wadell, *Shape Determinations of Large Sedimental Rock-Fragments*, Pan-American Geologist **61**, 187 (1934). Unfortunately several misprints occur in this paper. The integration symbol, $\int$, is used throughout the paper instead of f as symbol for function. Eq. (8) on page 203 should read: $\Psi=d_n/D_S+0.1$.

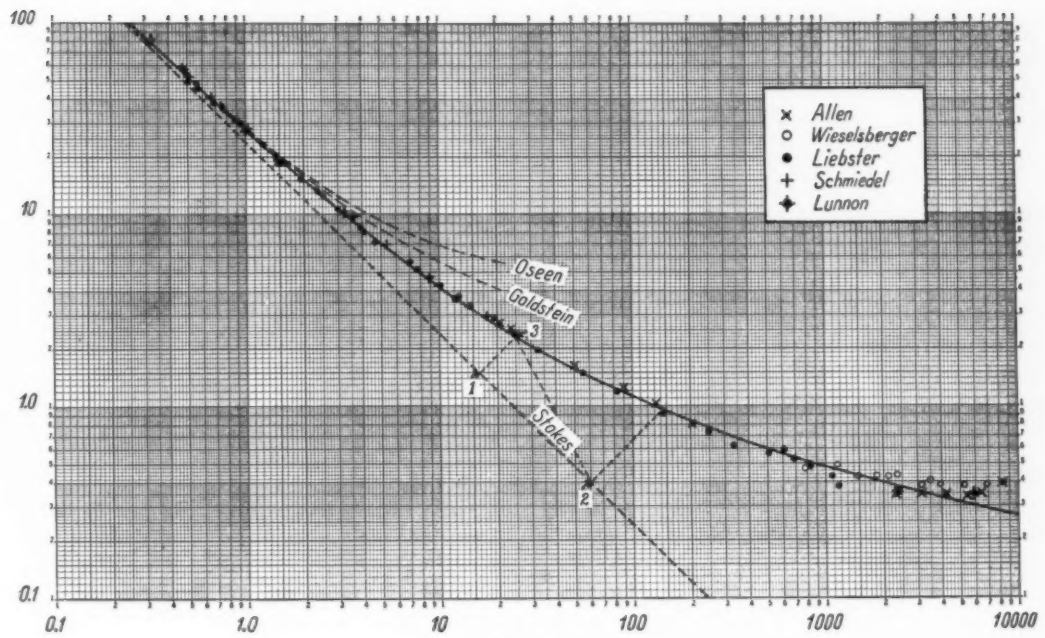

FIG. 5.

TABLE I.

Solid No.	Geometric shape classification	ψ	$th.$ cm	r_d cm	r_n cm	r_{sSt} or r_s cm	Volume cc $((4/3)\pi r_n^3)$	Material	ρ_S	ρ_F	μ	ν	v cm/sec.	R	C_R
1	Circular disk (Schmiedel 13)	0.1219	0.02068	0.99900	0.24922	0.07176	0.064837	Steel	7.674	1.199	0.4417	0.3684	11.55	15.627	26.393
2	Circular disk (Schmiedel 1)	0.2182	0.01050	0.20255	0.06862	0.04127	0.0013533	Steel	7.674	1.223	1.7012	1.391	1.408	0.1389	477.60
3	Circular disk (Schmiedel 10)	0.2182	0.010497	0.20250	0.06860	0.02843	0.0013523	Steel	7.674	1.150	—	0.0906	7.569	11.46	17.77
4	Circular disk (Pernolet 5)	0.2375	0.125	2.100	0.74495	0.060463	1.7318	Lead	11.150	0.9986	—	0.0106	56.2	7881.	6.269

All values above refer to the tardiest shape position, i.e., with the flat face of the disk normal to the direction of translation. Table I shows that $r_d > r_n > r_s$. It is interesting to note that the difference between the true nominal radius and the sedimentation radius is comparatively slight at low Reynolds numbers. Thus the actual size of a very flat particle, even in the tardiest position, can be determined with a fair accuracy by the sedimentation method, *when Stokes' law is applicable*, i.e., below Reynolds number 0.2. If the effective weight of a particle in water as sedimentation medium is so high that Stokes' formula is not applicable, the sedimentation can be brought within the validity of Stokes' law, either by employing heavy liquids, thereby reducing the effective weight, the settling velocity and the Reynolds number, or else by using liquids of high viscosity with practically the same result, namely, reduced velocity and lower Reynolds number. These methods apply to investigations, the aim of which is to obtain a size determination of highest possible accuracy for non-spherical particles.

COMPUTATION OF THE SEDIMENTATION RADIUS

Method I

The data presented in the preceding section showed that the size of the sedimentation radius departs from that of the true nominal radius with increasing Reynolds number. For many practical purposes it is, however, of interest to obtain a size classification of granular substance by sedimentation or elutriation in air or water,

although the computed size values depart from the actual ones with increasing **R**-values. Only when dealing with perfect spheres is the true volume size obtained, because then the actual radius, r_a, equals r_s and r_n. Stokes' or Oseen's well-known formulas, the validity of the latter extending to an **R**-value of about 0.5, are used for lower Reynolds numbers. A recent improvement by Goldstein[17] carries the validity of his formula but slightly above Reynolds number 0.5. Zahm's[18] equation for the coefficient of resistance for spheres at higher Reynolds numbers is valid between **R**-values ranging between approximately 1000 and 0.3, but, instead of gradually merging with the linear function of Stokes' law, the curve constructed on his formula departs from Stokes' law in an increasing degree with decreasing Reynolds. This deviation, as well as the fact that the radius must be known in order to compute the value of the coefficient of resistance, makes Zahm's formula unsuitable for sedimentation purpose. There are several empirical formulas which hold approximately for higher Reynolds numbers, but they are usually not confined to any special shape and disregard the influence of the form under the author's assumption that the shape variation of sedimentary particles is slight, or else they fail to bridge satisfactorily the region between the upper limit for the validity of Stokes' law and higher Reynolds numbers.

Every factor in Eqs. (2) and (3) must be known in order to determine the $C_R=f(\mathbf{R})$ in the logarithmic chart. The size of the sedimentation radius can, however, be determined without knowing the size of the true nominal radius. An inspection of Eqs. (2) and (3) discloses that the true nominal radius, r_n, enters both formulas. By combining the two into a ratio, o, the true nominal radius, r_n, is eliminated:

$$o=C_R/\mathbf{R}=4(\rho_S-\rho_F)g\nu/3v^3\rho_F. \qquad (4)$$

We assume that a disk-shaped particle No. 1 and a spherical particle No. 2 have the same specific gravity and the same terminal uniform settling velocity in the same fluid. Thus all properties of the two sedimentation systems are the same, except the true nominal radii of the two solids, which we can suspect to differ on account of the same velocity of the two solids, but the relative great difference in shape between a sphere and a disk. Since the true nominal radius, r_n, is eliminated in the ratio o, and because all the other properties of the two systems are the same, we conclude that the ratio o_1 of the disk equals o_2 of the sphere. Since the velocities of the two solids were assumed to be the same, we can formulate the following thesis:

Thesis I. *All solids of the same specific gravity, irrespective of their volume sizes, shapes or shape positions, have the same terminal uniform settling velocity in the same fluid, when the ratio of the coefficient of resistance to the Reynolds number for respective solids has the same numerical value.*

The sedimentation radius can be determined graphically on the basis of this thesis. All solids, which according to their $C_R=f(\mathbf{R})$ coincide with the linear function $y=x$ or $C_R=\mathbf{R}$, in the special case of chart Fig. 4, must have the same terminal settling velocity under the provisions of Thesis I, because the ratios y/x or $C_R/\mathbf{R}$ have the same numerical value, i.e., *one*. The same relationship exists between solids, the $C_R=f(\mathbf{R})$ of which coincide with any other straight line parallel to $y=x$. Consequently, disk No. 1 (chart Fig. 4) on line a to $b\,||\,y=x$ has the same terminal velocity and the same sedimentation radius as a sphere No. 2 on the same line and on the experimentally constructed curve for spheres.

The data required for our numerical illustration have been obtained from Schmiedel.[9] Dot No. 1 in chart Fig. 4 represents the $C_R=f(\mathbf{R})$ for a disk of steel ($\psi=0.1219$) in its tardiest shape position. The coefficient of resistance and the Reynolds number have been computed according to Eqs. (2) and (3). The numerical values are given in Table I, solid No. 1 (Schmiedel 13). In order to construct a case in analogy with ordinary sedimentation methods, we assume that the $C_R=f(\mathbf{R})$ and the true nominal radius of the disk are not known. We compute the ratio o_1 for the disk by applying Eq. (4) and substituting the numerical values of Table I.

---

[17] S. Goldstein, *The Steady Flow of Viscous Fluid Past a Fixed Spherical Obstacle at Small Reynolds Numbers*, Proc. Roy. Soc. (London) **A123**, 225 (1929).

[18] A. F. Zahm, *Flow and Drag Formulas for Single Quadrics, Twelfth Annual Report of the National Advisory Committee for Aeronautics, 1926*, Report No. 253, pp. 517–537.

$$o_1=\frac{4(7.674-1.199)981\cdot 0.3684}{3\cdot(11.55)^3\cdot 1.199}=1.6889. \quad (5)$$

Table I shows that $C_R=26.393$ and $\mathbf{R}=15.627$, $\therefore\ C_R/\mathbf{R}=26.393/15.627=1.6889$, which is the same numerical value obtained by Eq. (5). The numerical value of o_1 does not permit any determination of the $C_R=f(\mathbf{R})$, but we know that, if the numerical value of o for any other solid equals that of o_1 under the provision of Thesis I, then this solid has the same terminal velocity as the disk. In order to construct the line *a to b* we choose an arbitrary coefficient of resistance, for instance, $C_R=40$, and determine the $C_R=f(\mathbf{R})$ and the Reynolds number for a point *a* of the same numerical *o*-value as the disk. Thus $40/\mathbf{R}=1.6889$, $\therefore\ \mathbf{R}=23.68$. The cross-mark *a* in chart Fig. 4 is located by $C_R=40$ and $\mathbf{R}=23.68$. We can now either draw a line $||y=x$, or locate a point *b* in the same manner as point *a* was obtained. The line *a to b* crosses the experimentally constructed curve for spheres at a point No. 2, which is the $C_R=f(\mathbf{R})$ for a sphere of the same terminal velocity as the disk, i.e., the *sedimentation sphere* of the disk. Reynolds number 4.50 for point No. 2 is determined at the lower margin (*x*-axis) of the chart. The sedimentation radius, r_s, can now be computed by Eq. (3). Substituting the numerical values of Table I and inserting r_s instead of r_n in Eq. (3), we find that:

$$4.50=(2\cdot r_s\cdot 11.55)/0.3684, \quad (6)$$
$$\therefore\ r_s=0.071767 \text{ cm.}$$

The accuracy of the obtained value of r_s depends on the exactness of the reading of the Reynolds number on the chart. However, even a crude determination of the **R**-value is satisfactory, because the variation of the experimental data, upon which the curve for spheres is based, permits a sufficient range in variation of the determined Reynolds number (see Fig. 5).

Method II

The well-known equation for the *Stokes radius*, r_{St}, and the *Stokes velocity*, v_{St}, read:

$$r_{St}=[9\mu v/2(\rho_S-\rho_F)g]^{\frac{1}{2}}. \quad (7)$$

$$v_{St}=2r^2(\rho_S-\rho_F)g/9\mu. \quad (8)$$

For spherical shapes within the region of Stokes' law the actual radius, r_a, equals the Stokes radius, r_{St}, and the Stokes velocity, v_{St}, equals the actual velocity, v_a. For non-spherical solids in the tardiest position the true nominal radius, r_n, is always larger than the Stokes sedimentation radius, r_{sSt}, computed according to Eq. (7). For **R**-values higher than 0.2, $r_{St}<r_a$ for spherical shapes, and for non-spherical forms in the tardiest position $r_{sSt}<r_n$, and $r_s<r_n$, r_s representing the sedimentation radius computed according to Method I.

The linear function of Stokes' law is expressed by the equation $C_{RSt}=24/\mathbf{R}_{St}$, where C_{RSt} represents the *Stokes coefficient of resistance* and $\mathbf{R}_{St}$ is the *Stokes Reynolds number*. The formula is obtained by inserting Stokes' well-known expression for the resistance in the conventional formula for C_R:

$$C_R=\frac{R}{\pi r^2(v^2\rho_F)/2};\quad C_{RSt}=\frac{6\pi\mu r_{St}v_{St}}{\pi r_{St}^2(v_{St}^2\rho_F)/2},$$

$$\therefore\ C_{RSt}=\frac{12\mu}{r_{St}v_{St}\rho_F}. \quad (9)$$

$$\mathbf{R}_{St}=2r_{St}v_{St}\rho_F/\mu=2r_{St}v_{St}/\nu. \quad (10)$$

$$C_{RSt}\mathbf{R}_{St}=24,\quad \therefore\ C_{RSt}=24/\mathbf{R}_{St}. \quad (11)$$

Since $r_{St}<r_a$ and $v_{St}>v_a$ for Reynolds numbers higher than 0.2, Eq. (11) cannot, strictly speaking, be employed for computing the Stokes coefficient of resistance for higher **R**-values, because the numerical values of r_a and v_a have not the same relation to each other as r_{St} and v_{St}, the latter being in agreement with Stokes' law, according to which the square of the radii is proportional to the velocities. Eq. (11), or rather a similar one, $C_R=24/\mathbf{R}$, has, however, frequently been used for computing the Stokes coefficient of resistance for higher **R**-values, with the purpose of showing the amount of deviation of the Stokes coefficient of resistance from the actual one, C_{Ra}. Since $r_{St}<r_a$, $v_{St}>v_a$, $C_{RSt}<C_{Ra}$, for Reynolds numbers higher than 0.2, we have really two different conceptions involved, namely, the $C_{RSt1}=f(\mathbf{R}_{St1})$ corresponding to $C_{Ra}=f(\mathbf{R}_a)$ on the basis of $v_{St}=v_a$, and the $C_{RSt2}=f(\mathbf{R}_{St2})$, which corresponds to $C_{Ra}=f(\mathbf{R}_a)$ on the basis that $r_{St}=r_a$.

$$\because v_{St}=v_a, \quad \therefore C_{RSt1}=12\mu/r_{St}v_a\rho_F. \tag{12}$$

$$\because v_{St}=v_a, \quad \therefore \mathbf{R}_{St1}=2r_{St}v_a\rho_F/\mu = 2r_{St}v_a/\nu. \tag{13}$$

$$C_{RSt1}=24/\mathbf{R}_{St1}. \tag{14}$$

$$\because r_{St}=r_a, \quad \therefore C_{RSt2}=12\mu/r_a v_{St}\rho_F. \tag{15}$$

$$\because r_{St}=r_a, \quad \therefore \mathbf{R}_{St2}=2r_a v_{St}\rho_F/\mu = 2r_a v_{St}/\nu. \tag{16}$$

$$C_{RSt2}=24/\mathbf{R}_{St2}. \tag{17}$$

Since $v_a<v_{St}$ and $r_a>r_{St}$, hence $C_{Ra}>C_{RSt1}>C_{RSt2}$ and $\mathbf{R}_{St1}<\mathbf{R}_a<\mathbf{R}_{St2}$. The conceptions are graphically demonstrated in chart Fig. 5, where dot No. 3 represents the $C_{Ra}=f(\mathbf{R}_a)$ for a sphere, and dots Nos. 1 and 2 represent $C_{RSt1}=f(\mathbf{R}_{St1})$ and $C_{RSt2}=f(\mathbf{R}_{St2})$, respectively, for the same sphere in the same fluid. Our aim is to show that the actual radius, r_a, and the actual sedimentation radius, r_s, can be determined graphically by correction of the Stokes radius, r_{St}, and the Stokes sedimentation radius, r_{sSt}. We have chosen a numerical illustration as the simplest manner of demonstrating the method.

Applying Eq. (7) and substituting the numerical values of Table I, solid No. 1 (Schmiedel 13), we find that the Stokes sedimentation radius, r_{sSt}, for the disk amounts to,

$$r_{sSt}=\frac{9\cdot 0.4417\cdot 11.55}{2(7.674-1.199)981}=0.06012 \text{ cm}. \tag{18}$$

Next we determine the Reynolds number, $\mathbf{R}_{St1}$, for the Stokes sedimentation radius by formula No. 13, and substituting numerical values:

$$\mathbf{R}_{St1}=(2\cdot 0.06012\cdot 11.55)/0.3684=3.7697. \tag{19}$$

We can now compute the Stokes coefficient of resistance, C_{RSt1}, by Eq. (14).

$$C_{RSt1}=24/3.7697=6.367. \tag{20}$$

Dot No. 3 in chart Fig. 4 has a $C_{RSt1}=6.367$ and a $\mathbf{R}_{St1}=3.7697$, thus located on the point where the linear function of Stokes' law crosses the line *a to b*, the latter crossing the experimentally constructed curve at a point No. 2, i.e., the point which by Method I was determined as the $C_{Ra}=f(\mathbf{R}_a)$ for the disk's sedimentation sphere of radius r_s. The construction of the line *a to b* and subsequent computations are the same as in Method I. Thus we find that $r_s=0.07176$ cm, which is the same numerical value obtained by Method I.

Computation of the Actual Radius of a Perfect Sphere and of the Sedimentation Radius

Method III

We have previously stated that the curve for spheres in Figs. 1, 2, 3 and 4 was constructed on the basis of experimental data, corrected by Ladenburg's formula for the influence of the wall of the sedimentation vessel. The value of the computed sedimentation radius refers there-

Table II.

I $\mathbf{R}_{St1}$	II C_{RSt1}	III C_{Ra}	IV $\mathbf{R}_a$
0.010	2400.00	2407.68	0.01003
0.100	240.00	243.84	0.1016
0.250	96.00	98.91	0.2575
0.300	80.00	82.75	0.3103
0.350	68.57	71.20	0.3634
0.400	60.00	62.52	0.4168
0.500	48.00	50.36	0.5246
0.600	40.00	42.29	0.6335
0.700	34.28	36.42	0.7436
0.800	30.00	32.05	0.8547
0.900	26.66	28.64	0.9668
1.000	24.00	25.92	1.080
1.500	16.00	17.69	1.659
2.000	12.00	13.55	2.259
2.500	9.600	11.05	2.879
3.000	8.000	9.379	3.517
4.000	6.000	7.264	4.843
5.000	4.800	5.982	6.232
6.000	4.000	5.119	7.679
7.000	3.428	4.497	9.182
8.000	3.000	4.026	10.73
9.000	2.666	3.657	12.34
10.00	2.400	3.360	14.00
15.00	1.600	2.449	22.96
20.00	1.200	1.979	32.98
25.00	0.9600	1.688	43.97
30.00	0.8000	1.489	55.86
40.00	0.6000	1.232	82.16
50.00	0.4800	1.071	111.6
60.00	0.4000	0.9597	143.9
70.00	0.3428	0.8772	179.1
80.00	0.3000	0.8133	216.8
90.00	0.2666	0.7621	257.2
100.0	0.2400	0.7200	300.0
150.0	0.1600	0.5848	548.2
200.0	0.1200	0.5096	849.3
250.0	0.09600	0.4602	1198.6
300.0	0.08000	0.4248	1593.1
400.0	0.06000	0.3762	2508.2
500.0	0.04800	0.3436	3580.0
600.0	0.04000	0.3199	4798.3
700.0	0.03428	0.3014	6155.2
800.0	0.03000	0.2866	7644.2
900.0	0.02666	0.2743	9260.8

fore to the corrected values for spheres. We shall in the following present a formula, by which the sedimentation radius and the actual radius of a perfect sphere can be computed directly, without graphic methods and on the basis of experimental data *without* Ladenburg's correction.

In chart Fig. 5 the dotted line, *1 to 3*, connecting the linear expression for Stokes' law with the experimentally constructed curve for spheres of *non-corrected* data, represents the ratio o of a given numerical value ($o=0.0914$). Thus a sphere of a radius r_{St1} (point No. 1, Fig. 5) must have the same terminal uniform settling velocity[19] ($v_{St1}=v_{a3}$) in the same fluid as a sphere of the same specific gravity and of an actual radius, r_{a3}; the $C_{Ra}=f(\mathbf{R}_a)$ of the latter sphere being located on the experimentally constructed curve at a point No. 3 of the same o-value as point No. 1. Since all properties of the "two sedimentation systems," except the radii, are the same, i.e., $\rho_{S1}=\rho_{S3}$, $\rho_{F1}=\rho_{F3}$, $\mu_1=\mu_3$, $g_1=g_3$, $v_{St1}=v_{a3}$, it follows that,

$$\frac{C_{Ra3}}{C_{RSt1}}=\frac{8r_{a3}(\rho_{S3}-\rho_{F3})g_3}{3v_{a3}^2\rho_{F3}}\times\frac{3v_{St1}^2\rho_{F1}}{8r_{St1}(\rho_{S1}-\rho_{F1})g_1}=\frac{r_{a3}}{r_{St1}}. \quad (21)$$

$$\frac{\mathbf{R}_{a3}}{\mathbf{R}_{St1}}=\frac{2r_{a3}v_{a3}}{\nu_3}\cdot\frac{\nu_1}{2r_{St1}v_{St1}}=\frac{r_{a3}}{r_{St1}}. \quad (22)$$

$$\therefore\ \mathbf{R}_{a3}/\mathbf{R}_{St1}=C_{Ra3}/C_{RSt1}. \quad (23)$$

It is possible to carry these equations a step further by determining the numerical constant of either $\mathbf{R}_a/\mathbf{R}_{St1}$ or C_{Ra}/C_{RSt1}. We have found by statistical methods that,

$$\mathbf{R}_a/\mathbf{R}_{St1}=1+0.08(\mathbf{R}_{St1})^{0.69897}. \quad (24)$$

$$\therefore\ \mathbf{R}_a=\mathbf{R}_{St1}[1+0.08(\mathbf{R}_{St1})^{0.69897}]. \quad (25)$$

$$\therefore\ C_{Ra}=C_{RSt1}[1+0.08(\mathbf{R}_{St1})^{0.69897}], \quad (26)$$

where the exponent $0.69897=\log 5$.

Column I of Table II gives successive numbers of $\mathbf{R}_{St1}$, and column II gives corresponding C_{RSt1} according to Stokes' law, $C_{RSt1}=24/\mathbf{R}_{St1}$. Columns III and IV give the actual coefficient of resistance, C_{Ra}, and the actual Reynolds number, $\mathbf{R}_a$, respectively, for C_{RSt1} and $\mathbf{R}_{St1}$. The values of $\mathbf{R}_a$ and C_{Ra} have been computed according to Eqs. (25) and (26), respectively.

The solid curve in Fig. 5 illustrates the computed values of C_{Ra} and $\mathbf{R}_a$, expressed as $C_{Ra}=f(\mathbf{R}_a)$. The experimental data cluster round the curve with sufficiently close coincidence to verify the formulas. The curve merges with those of Oseen's and Goldstein's formulas at an **R**-value of about 0.5. It approaches the linear function of Stokes' law with decreasing Reynolds numbers, and, although the curve theoretically never crosses the Stokes line, it practically merges with the linear function of Stokes' law at an **R**-value of 0.01 (see Table II). The curve appears to depart somewhat from the experimental data at an **R**-value of about 3500. At these high Reynolds numbers ordinary sedimentation apparatus are too small for measuring the velocity in water. Ordinary sedimentary particles have, at this high **R**-value for water as sedimentation fluid, sufficient size to permit separate weight determination by ordinary laboratory balances. If, however, sedimentation methods are used for **R**-values above 10,000, the sedimentation radius can be computed by Method I.

The actual radius, r_a, of a sphere and the sedimentation radius, r_s, for a non-spherical solid can be computed in various ways. We have chosen the simplest method. Eqs. (13), (22) and (24) show that,

$$\mathbf{R}_a/\mathbf{R}_{St1}=r_a/r_{St1}=1+0.08(\mathbf{R}_{St1})^{0.69897}.$$

Hence,

$$r_s=r_a=r_{St}[1+0.08(2r_{St}v_a\rho_F/\mu)^{0.69897}], \quad (27)$$

where

$$r_{St}=[9\mu v_a/2(\rho_S-\rho_F)g]^{\frac{1}{2}},$$

v_a is the observed, terminal uniform settling velocity, r_a the actual radius of a perfect sphere, and r_s the sedimentation radius for a non-spherical solid.

Table III gives the computed and measured radii of spheres for a range of Reynolds numbers down to an **R**-value of 0.0531, the latter being well below the upper limit for the assumed

[19] The reasoning above is based on the difference in the graphic positions of the two spheres, a difference due to the failure of Stokes' law for higher Reynolds numbers. The reasoning is not obscured by the fact $C_R=f(\mathbf{R})$ of all spheres really should coincide with the experimentally constructed curve.

TABLE III.

Data by	ρ_S	ρ_F	μ	Observed v_a cm/sec.	Reynolds number $\mathbf{R}_a$	Measured r_a cm	Computed r_a cm	(Stokes) r_{St} cm	Error % (Wadell)	Error % (Stokes)
Allen	7.666	0.99963	0.012735	100.5	3144.5	0.1993	0.2042	0.029676	+2.4	−85.1
Schmiedel	7.818	1.227	1.3718	36.24	17.922	0.27645	0.27081	0.18601	−2.03	−32.7
Schmiedel	2.700	1.228	1.6246	1.666	0.2437	0.09680	0.09448	0.091840	−2.39	− 5.12
Schmiedel	2.700	1.233	1.9987	1.370	0.1636	0.09680	0.09455	0.092530	−2.32	− 4.41
Schmiedel	7.524	1.233	2.0452	1.703	0.1059	0.05045	0.05122	0.05040	+1.52	− 0.09
Schmiedel	2.700	1.228	1.5939	0.6109	0.0531	0.05655	0.05564	0.055085	−1.60	− 2.59

validity of Stokes' law. The data, illustrating the *general* difference between the results obtained by Eq. (27) and by use of Stokes' law, refer to spheres, the $C_R=f(\mathbf{R})$ of which coincide as close as possible with the constructed curve. The difference between the computed and measured radii is expressed as an "error," computed as percentage of the value of the measured radius. The plus sign (+) shows that the computed radius is larger than the measured one, and the minus sign (−) indicates that the former is smaller than the latter. The table shows that even in the vicinity of and below Reynolds number 0.2 the formula presented in this paper gives results, which agree well with the experimental data.

A New Resistance Formula for Spheres

For convenience we repeat the conventional resistance formula for spheres:

$$R=\pi r_a^2(v_a^2\rho_F/2)C_{Ra}. \tag{28}$$

Eliminating C_{Ra} and substituting its equivalent given in Eq. (26):

$$R=\pi r_a^2(v_a^2\rho_F/2)\times C_{RSt}[1+0.08(\mathbf{R}_{St})^{0.69897}]. \tag{29}$$

Eliminating C_{RSt} and substituting its equivalent given in Eq. (12):

$$R=(\pi r_a^2 v_a^2\rho_F/2)\cdot(12\mu/r_{St}v_a\rho_F)\times[1+0.08(2r_{St}v_a\rho_F/\mu)^{0.69897}]. \tag{30}$$

Hence the following equation for the resistance, R;

$$R=6\pi\mu r_a v_a\cdot(r_a/r_{St})\times[1+0.08(2r_{St}v_a\rho_F/\mu)^{0.69897}], \tag{31}$$

where v_a is the observed terminal velocity, and r_{St} is computed in the same manner as in Eq. (27).

Computation of the Terminal Uniform Settling Velocity of a Sphere of a Radius Equal to the True Nominal Radius of a Given Non-Spherical Solid

By combining C_R and $\mathbf{R}$ (Eqs. (2) and (3)) into a product, $p=C_R(\mathbf{R})^2$, the velocity factor, v, is eliminated:

$$p=C_R(\mathbf{R})^2=32r_n^3(\rho_S-\rho_F)g/3\rho_F v^2. \tag{32}$$

We assume that a disk-shaped particle No. 1 and a spherical particle No. 4 have the same true nominal radius and the same specific gravity, and that they are settling in the same fluid. Thus all properties of the two sedimentation systems are the same, except that the shapes of the solids differ and the terminal velocities are not known. Applying Eq. (32) we obtain two products, p_1 and p_4 for the disk and the sphere, respectively. Since the velocity factor is eliminated, and since all corresponding factors of p_1 and p_4 equal each other, we conclude that the product p_1 for the disk equals p_4 for the sphere. We can then formulate the following thesis:

Thesis II: *All solids of the same specific gravity settling in the same fluid, irrespective of their shapes, shape positions and terminal settling velocities, have the same true nominal radius or the same volume size, when the product $C_R(\mathbf{R})^2$ of respective solids has the same numerical value.*

In chart Fig. 4 we have a straight line representing the equation $y=100/x^2$, or in the special case of this chart, $C_R=100/\mathbf{R}^2$, hence, $C_R(\mathbf{R})^2=100$. Consequently, all solids the $C_R=f(\mathbf{R})$ of which coincide with the line $y=100/x^2$ must have the same numerical p-value, i.e., $p=C_R(\mathbf{R})^2=100$, and they must therefore also have the same true nominal radius, r_n, under the provisions given in Thesis II. The same relationship exists between solids, the $C_R=f(\mathbf{R})$ of which

coincide with any other straight line $||\ y = 100/x^2$.

We have chosen a numerical illustration as the simplest method of demonstrating the computation of the terminal velocity for a sphere of a radius equal to the true nominal radius of a given non-spherical solid. Dot No. 1 in chart Fig. 4 represents the $C_R = f(\mathbf{R})$ for a circular disk of steel in its tardiest shape position. The known properties of the sedimentation system are, r_n, ρ_S, ρ_F, and ν. Applying Eq. (32) and substituting the numerical values of Table I, solid No. 1 (Schmiedel 13):

$$P_1 = \frac{32 \cdot (0.24922)^3 \cdot (7.674 - 1.199)981}{3 \cdot 1.199 \cdot (0.3684)^2} = 6445. \quad (33)$$

If the numerical p-value of any other solid equals p_1 under the provisions given in Thesis II, then this solid must have the same true nominal radius as the disk. We choose an arbitrary coefficient of resistance, for instance, $C_R = 40$, and then determine the Reynolds number for this solid h:

$$p_1 = 6445 = 40(\mathbf{R})^2, \quad \therefore \mathbf{R} = 12.69. \quad (34)$$

The cross-mark h in chart Fig. 4 represents the solid h of $C_R = 40$, and $\mathbf{R} = 12.69$. This solid must have the same true nominal radius as a sphere of a radius equal to the true nominal radius of the disk. It follows also that the $C_R = f(\mathbf{R})$ of the disk and of the sphere must coincide with a straight line passing through $h\,||\,y = 100/x^2$. In construction of such a line we choose an arbitrary coefficient of resistance, for instance, $C_R = 3$, and determine the point q in the same manner as h was located. We extend the line h *to* q till it crosses the experimentally constructed curve for spheres at a point No. 4. The Reynolds number for this point may be read at the lower margin (x-axis) of the chart. Having found that the Reynolds number for sphere No. 4 amounts to 72, we can compute the terminal velocity for this sphere. Applying Eq. (3) and substituting the numerical values of Table I:

$$\mathbf{R} = 72 = 2 \cdot 0.24922 \cdot v_a / 0.3684, \quad \therefore v_a = 53.216 \text{ cm/sec.} \quad (35)$$

We have thus arrived to the result that a sphere of the same volume size and of the same specific gravity as the disk has a terminal uniform settling velocity of 53.216 cm/sec. in the same fluid. This velocity is about 4.6 times greater than that of the disk (11.55 cm/sec.) in its tardiest shape position.

The actual velocity can also be computed by correction of the Stokes velocity on the basis of the same reasoning presented above.

Thermal Agitation Voltages in Resistors

C. NEITZERT, *Massachusetts Institute of Technology, Round Hill Research Division, Department of Electrical Engineering*

(Received April 2, 1934)

The limited range of previous measurements of thermal agitation voltage is pointed out and data are given which extend the range of resistances and frequencies considerably. The results substantiate Nyquist's theory for resistances up to 1.7×10^{9} ohms and for frequencies between 1 and 10,000 cycles per second. A value of 1.366×10^{-16} ergs per degree with a probable error of 0.016×10^{-16} ergs per degree is obtained for Boltzmann's constant. This is nearer to the accepted value than previous determinations by this method have given.

FOR some years it has been known that the thermal motion of electrons in conductors gives rise to a voltage across the terminals of the conductor. The effect was discovered and first studied by J. B. Johnson.[1] This voltage may, in the case of a high-gain amplifier, be sufficiently large to mask the voltage to be measured and therefore determine the lower limit of measurements. It is the purpose of this paper to discuss the effect and its relation to the problem of high-gain amplification and to present additional data as to its nature.

The nature of the phenomenon may be easily explained in very simple words. In every conductor there exists free electrons. These electrons, because of their thermal energy, are in a continual state of agitation. The movement of these electrons constitutes a current, and when a current flows through a resistance a difference of potential exists across the resistance.

Certain characteristics may be immediately pointed out upon the recognition of the existence of the effect. First, the voltage is a random voltage since it is caused by the random motion of the electrons. Second, the average value of the voltage over a sufficiently long period of time is zero because there is no general trend to the motion of the electrons, that is, there is no piling up of the charge at any point in the conductor. Third, the voltage is a function of the temperature and the resistance.

By assuming that the ordinary laws of conduction hold, it is possible to obtain additional data on this effect. Consider two resistances R_1 and R_2 of any magnitude, physical size, shape or composition connected as shown in Fig. 1. Let $\overline{e_1^2}$ be the mean-square voltage generated in resistor R_1 and $\overline{e_2^2}$ that generated in R_2. By virtue of the voltage generated in R_1 a current

$$i_1=\overline{e_1^2}/(R_1+R_2) \tag{1}$$

will flow in the circuit. The rate at which energy from R_1 is dissipated in R_2 is

$$P_1=i_1^2R_2=\overline{e_1^2}R_2/(R_1+R_2)^2. \tag{2}$$

Similarly, the rate at which energy from R_2 is dissipated in R_1 is

$$P_2=i_2^2R_1=\overline{e_2^2}R_1/(R_1+R_2)^2. \tag{3}$$

But, in order that there be no net energy transfer, that is, that one resistor shall not be cooled and the other heated, these powers must be equal and $\overline{e_1^2}R_2=\overline{e_2^2}R_1$, or

$$\overline{e_1^2}/\overline{e_2^2}=R_1/R_2. \tag{4}$$

We therefore conclude that, if the ordinary laws of conduction hold, the mean-square value of the voltage is directly proportional to the resistance and is independent of the physical size, shape, and composition of the resistor. H. Nyquist,[2] by replacing R_2 of Fig. 1 by a complex impedance R_f+jX_f and providing that there be no net energy transfer, has shown that for a complex impedance the mean-square voltage is proportional to the real part of the impedance. In amplifiers the principal circuit encountered is that of a resistance and capacitance in parallel, the capacitance being that of the circuit leads and of the tube. For such a circuit the real part of the impedance is

$$R(f)=R/(1+R^2C^2\omega^2). \tag{5}$$

[1] Johnson, Phys. Rev. **32**, 97 (1928).

[2] Nyquist, Phys. Rev. **32**, 110 (1928).

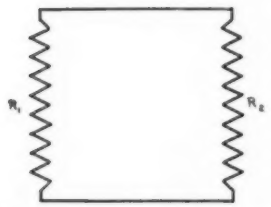

FIG. 1. Circuit for showing the variation of resistance noise with resistance.

J. B. Johnson's[1] work indicated that the mean-square voltage was proportional to the temperature and the resistance and independent of the frequency except insofar as the frequency affected the resistance. Since an amplifier is required to measure the voltage it becomes convenient to express the effect in terms of the output current in an amplifier. Johnson found that if $Y(f)$ is the conductance function of the amplifier the output current is expressed by

$$\overline{i^2}=4kT\int_0^\infty R(f)\,|\,Y(f)\,|^2 df, \qquad (6)$$

where k is Boltzmann's constant and T is the absolute temperature. His measurements covered temperature from -180°C to 100°C, frequencies from 300 to 2000 cycles per second, and resistances up to almost one megohm. Using Eq. (6) he obtained a value of 1.27×10^{-16} ergs per degree for Boltzmann's constant. H. Nyquist[2] developed a theoretical formula and also arrived at Eq. (6).

H. D. Ellis and E. B. Moullin[3] used the effect as a means of determining Boltzmann's constant, assuming Eq. (6) to be correct. Their measurements were principally limited to two values of resistance, 62,000 and 110,000 ohms, and covered the frequency range between 1700 and 3300 cycles per second. They give values of Boltzmann's constant ranging from 1.35×10^{-16} to 1.361×10^{-16} ergs per degree.

E. K. Sandeman and L. H. Bedford[4] made measurements with resistances between 10^4 and 10^6 ohms but for wide-frequency band. In one case they used a band between 30 and 7000 cycles per second and in another case a band between 30 and 2200 cycles per second.

Williams and Wilbur[5] reports measurements made at boiling water and liquid air temperatures but are not clear as to the range of resistance and frequency covered.

Although the above researches give good checks on the theory, their range is somewhat limited. The use of comparatively small resistances and low frequencies made it unnecessary to take into account the variation of resistance with frequency. In addition, work reported by Thatcher[6] seemed to indicate that the theory did not hold for higher resistances. It was also thought possible that an abnormal effect might occur at very low frequencies as in the case of the small shot effect.

Measurements were therefore made for resistances between 1×10^3 and 1.7×10^9 ohms and at frequencies between 1 and 10,000 cycles per second. The measuring circuit was arranged to make the shunt capacitance as small as possible. This was desirable since the size of the capacitance determines the range of resistance that may be measured at a given frequency. Curve I of Fig. 2 gives $R(f)/R=1/(1+R^2C^2\omega^2)$ as a function of $RC\omega$. For values of $RC\omega$ less than 0.1, $R(f)$ is equal to R to within 1 percent.

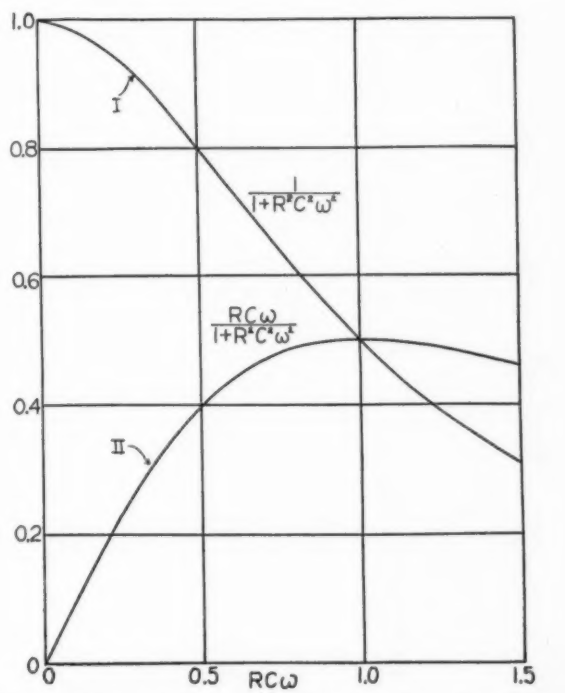

FIG. 2. Variation of the resistance of a parallel $R-C$ circuit with frequency and d.c. resistance.

[1] Ellis and Moullin, Proc. Phil. Soc. **28**, 386 (1932).
[2] Sandeman and Bedford, Phil. Mag. **7**, 774 (1929).
[3] Williams and Wilbur, Science **76**, 519 (1932).
[4] Thatcher, Phys. Rev. **40**, 121 (1932).

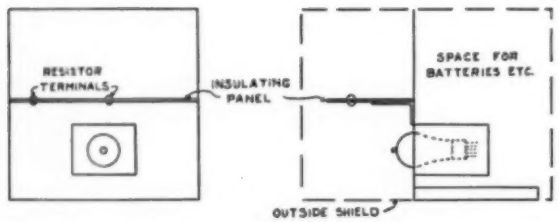

FIG. 3. Arrangement of the first stage and resistor mounting.

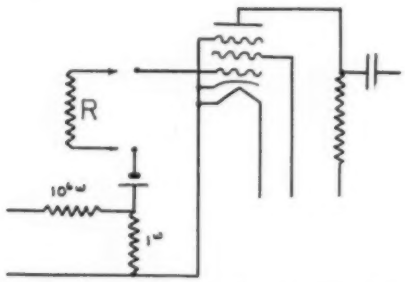

FIG. 4. Circuit diagram of the first stage and calibration circuit.

However, for values of $RC\omega$ greater than 0.1, $R(f)$ may be considerably different from R. Curve II of Fig. 2 gives $R(f)C\omega$ as a function of $RC\omega$ or $R(f)$ as a function of R for a fixed capacitance and frequency. It reaches its maximum value when $RC\omega=1$ or when $R=1/C\omega$, and at this point $R(f)=0.5\ 1/C\omega$. The maximum resistance obtainable at a given frequency is therefore determined by the input capacitance of the amplifier. Fig. 3 shows the physical arrangement of the first stage. The input capacitance as measured on an impedance bridge was 13 micromicrofarads.

The amplifier used was an ordinary resistance-capacitance coupled amplifier having a tuned circuit in the plate circuit of one stage. The first stage was located in a separate shielded box with the measuring circuit. Fig. 4 is a schematic diagram of the first stage showing the arrangement of the resistor upon which measurements were made and of the calibration circuit.

Errors in the calibration circuit due to shunt capacitance were eliminated by shielding. Fig. 5 is a schematic diagram of the calibration circuit showing the shunt capacitances and the impedance R_L of the cable from the voltmeter.

Condenser C_1 causes an error only because of the additional current it draws through R_L. Since R_L is only a small fraction of an ohm, this error is negligible. Condenser C_2 is in parallel

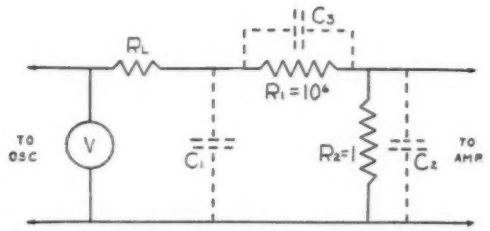

FIG. 5. True diagram of the calibration circuit.

with 1 ohm and would have to be two microfarads in order to cause an error of 1 percent at 10,000 cycles per second. Condenser C_3 is in parallel with 1 megohm and is apt to cause an error at high frequencies unless it is made small. By shielding R_1 from R_2, C_3 may be reduced to the self-capacitance of R_1. Wire-wound resistors having a self-capacitance of about two micromicrofarads may be used with an error of less than 1 percent for frequencies up to 10,000 cycles per second. By shielding R_1 and the cable to the amplifier, errors due to inductive coupling are eliminated.

The output of the amplifier was fed into a thermal meter so that the root-mean-square value of the output current could be read.

Johnson's data were considered sufficient evidence of the relation of the voltage to temperature so that measurements were made only at 300° absolute with a probable error of 1°.

Measurements were carried out on the assumption that the present theory did not hold so that precautions were taken to eliminate reliance on the formula of Eq. (6). It was assumed that the voltage was a function of only the resistance, the temperature and the frequency. Then in the small increment of frequency between f and $f+df$ the current in the output of the amplifier would be given by

$$d\bar{i}^2=F[R(f),\ T,f]\,|\,Y(f)\,|^2df, \qquad (7)$$

and the total current is given by

$$\bar{i}^2=\int_0^\infty F(R(f),\ T,f)\,|\,Y(f)\,|^2df. \qquad (8)$$

Now if the amplifier is tuned very sharply, F may be considered constant over the frequency range that contributes appreciably to $\bar{i}^2$ and Eq. (8) becomes

$$\bar{i}^2=F(R_0,\ T,f_0)\int_0^\infty |\,Y(f)\,|^2df, \qquad (9)$$

where R_0 and f_0 are the values of $R(f)$ and f at which $Y(f)$ is a maximum. The band width varied from about 10 cycles at 10,000 cycles per second to about 1 cycle at 30 cycles per second as compared with band widths ranging between 200 and 400 cycles used by Ellis and Moullin.

Now on the assumption that $\overline{i^2}$ is proportional to T Eq. (9) becomes

$$\overline{i^2}=G(R_0, f_0)T\int_0^\infty |Y(f)|^2 df. \qquad (10)$$

The method of measurement consisted in tuning the amplifier to a given frequency and then reading the current for a series of resistances up to 250 megohms, and also for zero resistance. The conductance function, $|Y(f)|$, was then obtained by applying a variable frequency known voltage to the calibration circuit. After correction is made for the noise from the amplifier, the first of these readings gives a series of values of $\overline{i^2}$ in Eq. (10) for various values of R_0. The second gives the value of the integral* of Eq. (10). From these results we can obtain the value of G as a function of R_0 for a given frequency.

Fig. 6 shows $(\overline{i^2})^{\frac{1}{2}}$, of Eq. (10), typically plotted against R and Fig. 7 gives the corresponding curves of $|Y(f)|$ and $|Y(f)|^2$. The narrow band width was made possible by connecting a dynatron in parallel with the tuned circuit.

The slope of the curve of Fig. 6 is equal to 2 on the straight part of the curve, indicating that G varies directly as R_0, which would be indicated by Eq. (6). If the curved portion is to be accounted for by shunt capacitance, then the value of the capacitance may be calculated from the frequency and the resistance at which $(\overline{i^2})^{\frac{1}{2}}$ becomes a maximum. At this point $R=1/C\omega$ or $C=1/R\omega$. This gives $C=12.7$ micromicrofarads as compared to 13 micromicrofarads, the measured value. The solid line of Fig. 6 gives the theoretical value assuming that $\overline{i^2}$ varies as the real part of the impedance, that is, G of Eq. (10) is directly proportional to R_0. The only point that is off an appreciable amount is the one at 2.5×10^8 ohms and it is probably an experimental error.

Measurements were made at frequencies of approximately 30, 50, 100, 160, 250, 500, 780, 1000, 2000, 3000, 4000, 7000 and 10,000 cycles per second.

In addition to the above frequencies measurements were made at approximately 1 cycle per second and with resistances as high as 1.7×10^9 ohms using resistance capacitance tuning throughout the amplifier. The results at this frequency are not accurate because it was necessary to use a rectifying meter instead of a thermal meter in the output of the amplifier.

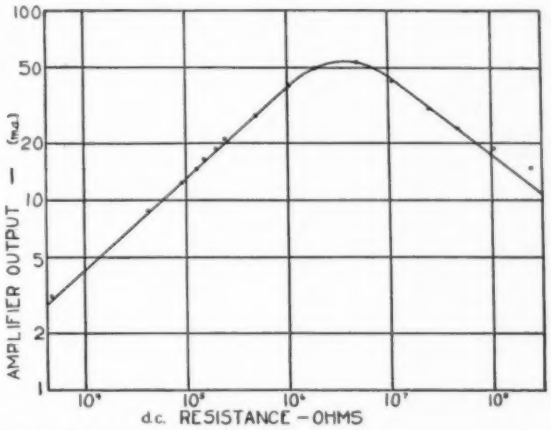

FIG. 6. Variation of the amplifier output current with the d.c. resistance of the circuit under test.

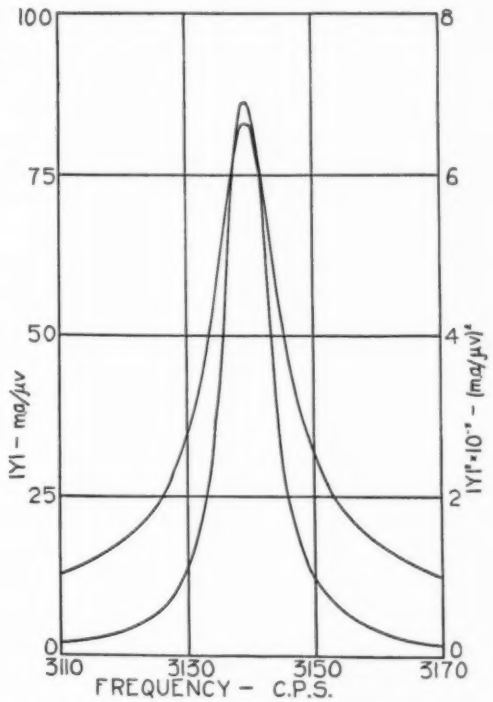

FIG. 7. The conductance and conductance squared of the amplifier for one frequency used.

* See appendix.

TABLE I.

Freq. for max. Y 1.	$\int \lvert Y(f)\rvert^2 df$ — (m.a./V)² Calculated 2.	Measured 3.	Total 4.	$\overline{(i^2)}$ — m.a. for $R_g = 10^6$ ohms 5.	$K \times 10^{16}$ 6.	Appar. input capacitance 7.
0.85	0	206	206	1.75	1.24	—
29.32	126	941	1067	4.24	1.41	—
51.53	26	467	493	2.79	1.31	—
100.66	80	1288	1368	4.74	1.37	13.3
159.46	590	7570	8160	11.2	1.28	13.3
250.66	4200	42000	46200	28.4	1.46	11.5
500.7	8200	87000	95200	40.3	1.42	12.7
773.3	8700	62300	71100	35.2	1.45	12.1
998.0	35000	212000	247000	60.4	1.23	12.3
2042.5	6500	635000	70000	34.8	1.44	13.0
3139.6	8900	90000	98900	40.4	1.38	12.7
3994.0	4200	100600	104800	41.0	1.34	13.5
7173.5	1100	52800	53900	26.3	1.07	13.0
10640.0	2800	45600	48400	28.0	1.35	12.5

However, the measurement is of sufficient importance to include with the other data as it indicates no change in the theory at very low frequencies.

Table I is a tabulation of the results at the various frequencies. Column 6 gives the value of Boltzmann's constant as computed from Eq. (6). By neglecting the values for 1 and 7000 cycles per second, these data give an average value of 1.366×10^{-16} erg per degree with a probable error of 0.016×10^{-16} erg per degree. Fig. 8 is a curve of k plotted against frequency. The points are scattered at random about the accepted value with no definite trend.

Column 7 of Table I gives the apparent input capacitance as computed from the value of d.c. resistance and the frequency for maximum $\overline{(i^2)}^{\frac{1}{2}}$.

These data seem to indicate that the present theory is true for the range of resistance and frequency covered in this research.

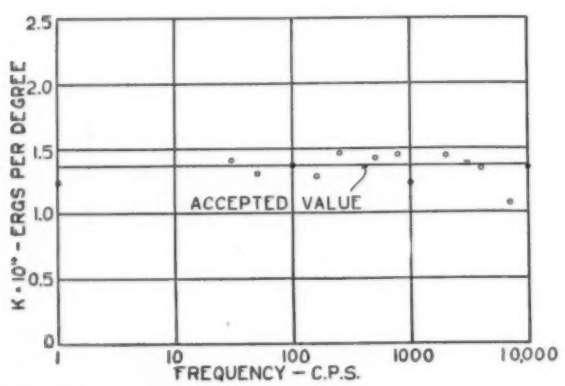

FIG. 8. The measured value of Boltzmann's constant as a function of frequency.

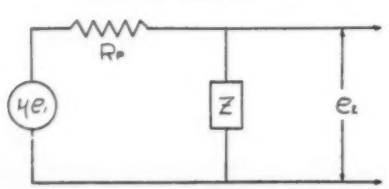

FIG. 9. Equivalent circuit of the stage containing the tuned circuit.

APPENDIX

Since the total area under the $|Y|^2 - f$ curve would have been very difficult to measure, the portion far removed from the resonant frequency was calculated by an approximate method.

In Fig. 9, R_p represents the plate resistance of the tube and Z the impedance of the tuned circuit. The voltage amplification of this circuit is

$$e_2/e_1 = \mu |Z|/|R_p + Z|. \tag{11}$$

If R_p is large, then sufficiently far from resonance $|Z| \ll R_p$ so that

$$e_1/e_2 = \mu |Z|/R_p \tag{12}$$

or is directly proportional to $|Z|$. Neglecting the error caused by the frequency characteristic of the remainder of the amplifier, it is true that $|Y|$ is also proportional to $|Z|$. By setting

$$|Z| = L\omega/(1 - LC\omega^2) = (Bf/f_0)/[1 - (f/f_0)^2] \tag{13}$$

we obtain

$$|Y| = B'x(f/f_0)/[1 - (f/f_0)^2]$$

and

$$\int |Y(f)|^2 df = \int \frac{(B'f/f_0)^2}{[1 - (f/f_0)^2]^2} df = B'^2 f_0 \int \frac{a^2 da}{(1 - a^2)^2}, \tag{14}$$

where $a = f/f_0$. This integral, when integrated between a_1 and a_2 gives

$$\int_{a_1}^{a_2} |Y(f)|^2 df = B'^2 f_0 \left[\frac{\frac{1}{2}a_2}{1 - a_2^2} - \frac{\frac{1}{2}a_1}{1 - a_1^2} + \tfrac{1}{4} \log \left(\frac{1 + a_1}{1 - a_1} \times \frac{1 - a_2}{1 + a_2} \right) \right] \tag{15}$$

$$= B'f^2_0 \left[\left(\frac{\frac{1}{2}a_2}{1 - a_2^2} - \tfrac{1}{4} \log \left| \frac{a_2 + 1}{a_2 - 1} \right| \right) - \left(\frac{\frac{1}{2}a_1}{1 - a_1^2} - \tfrac{1}{4} \log \left| \frac{a_1 + 1}{a_1 - 1} \right| \right) \right] \tag{16}$$

$$= B'^2 f_0 [F(a_1) - F(a_2)]. \tag{17}$$

Table II gives values of $a/1 - a^2$ and $F(a)$ for several values of a.

TABLE II.

a	$a/(1-a^2)$	$F(a)$	a	$a/(1-a^2)$	$F(a)$
0.60	0.94	0.12	1.01	50.3	23.8
.70	1.37	.25	1.02	25.2	11.46
.75	1.71	.37	1.03	16.9	7.41
.80	2.22	.56	1.04	12.7	5.39
.85	3.06	.90	1.05	10.2	4.19
.90	4.73	1.62	1.06	8.58	3.40
.92	5.99	2.21	1.08	6.49	2.39
.94	8.08	3.17	1.10	5.24	1.86
.95	9.75	4.00	1.15	3.57	1.12
.96	12.3	5.16	1.20	2.73	0.77
.97	16.4	7.16	1.30	1.88	.43
.98	24.8	11.2	1.40	1.46	.23
.99	49.7	23.5	1.60	1.03	.14

The Effect of Nascent Hydrogen on the Magnetic Properties of Iron*

R. K. REBER, *Sloane Physics Laboratory, Yale University*

(Received July 9, 1934)

Hydrogen was electrolyzed into flat ring cathodes of magnetically soft iron in 0.5 N solutions of H_2SO_4 or of KOH. The design of the electrolytic cell permitted magnetic testing at intervals. Magnetic hardening began after many hours provided the electrolytic current density was kept above a lower limit depending on the electrolyte. This hardening proceeded, at adequate current density, to an end point beyond which longer charging at any current density rarely produced any further changes in magnetic properties. Removal of hydrogen by storage in air at room temperature for 5 months, or by annealing at 400°C in vacuum for 17 hours, did not diminish the magnetic hardness produced during electrolysis. It is suggested that the iron is locally cold-worked by non-uniform distribution in it of hydrogen in excess of the solubility limit at room temperature, and that uniformly distributed hydrogen up to this limit has very little effect on the ferromagnetic properties.

HISTORICAL INTRODUCTION

NASCENT hydrogen (H_1^+) liberated in contact with iron in an acid bath, or by electrolysis, rapidly embrittles ordinary fine-grained metal. Such brittleness is relatively transient, even at room temperature.[1] Magnetic effects of such treatments are not striking and have not been studied in detail.[2]

The hardness of electrodeposited iron is usually ascribed to its retained hydrogen.[3] Removal of hydrogen by heating is accompanied by magnetic, as well as mechanical, softening.[4] It seems possible, however, to get out the hydrogen without much altering the hardness,[5] and the structure of such metal is so anisotropic that interpretation of magnetic changes in it is complicated at best. We do not consider electrodeposited iron further herein.

When this study was undertaken it seemed possible that the extreme magnetic softness of iron treated in hydrogen at very high temperatures by Cioffi[6] might, as he at first supposed, depend upon retained hydrogen. His later work[7] showed that the process is one of purification. Sieverts[8] is probably right in supposing that excess hydrogen is rapidly given up by iron at any annealing temperature. Such considerations as these led us to decide that the effects of hydrogen on the ferromagnetism of iron would prove easiest to interpret if produced at room temperature in the purest metal we could prepare in pieces suitable for magnetic testing. This limited us to electrolytic means and suggested careful purification by Cioffi's method as a standard preliminary process. As it seemed likely that transient effects might occur, means had to be provided for making magnetic measurements during electrolysis. Mechanical strains had to be avoided, since these may entirely alter the magnetic properties of soft magnetic materials. The saturation of iron with hydrogen at room temperature is a slow process.[9] It seemed, therefore, that very long times of experiment might be necessary, and that pieces of different thickness had better be studied under otherwise identical conditions. This sharply limited the number of materials we could hope to investigate.

---

* Condensed from a Dissertation presented to the Faculty of the Graduate School of Yale University in Candidacy for the Degree of Doctor of Philosophy.

[1] See e.g., L. B. Pfeil, Proc. Roy. Soc. **A112**, 182 (1926), and, most recently D. Alexejew, P. Afanassjew and W. Ostroumow, Zeits. f. Elektrochemie **40**, 92 (1934).

[2] D. E. Hughes, J. Soc. Telegraph Eng. **9**, 170, 178 (1880), detected no effect. H. Gries and H. Esser, Archiv f. Elektrot. **22**, 145 (1929), found 3 mm rods of soft iron slightly hardened, magnetically, by 30 min. in 0.5 N H_2SO_4 without current flow. J. Coulson, Phys. Rev. **19**, 528; **20**, 51 (1922) observed that the magnetic moments of steel bar magnet cathodes in 25 percent H_2SO_4 dropped by as much as 20 percent in some cases. He did not measure other magnetic properties.

[3] L. Cailletet, Comptes Rendus **80**, 319 (1875), showed hydrogen might be retained in large amount.

[4] C. F. Burgess and C. Hambuechen, Trans. Am. Electrochem. Soc. **5**, 201 (1904); R. Hugues, Rev. de métallurgie **22** [mém.], 764 (1925).

[5] Guichard, Clausmann, Billon and Lanthony, Comptes rendus **192**, 623, 1096; **193**, 1084 (1931).

[6] P. P. Cioffi, Nature **126**, 200 (1930).

[7] P. P. Cioffi, J. Frank. Inst. **212**, 601 (1931); Phys. Rev. **39**, 363 (1932).

[8] A. Sieverts, Zeits. f. Metallkde. **21**, 37 (1929).

[9] T. S. Fuller, Trans. Am. Electrochem. Soc. **36**, 113 (1919), found, for example, that hydrogen liberated continuously on one side of a 1.6 mm iron wall began to escape from the other side after upwards of 15 hours, but that no steady state of flow had been reached in 200 hours.

TABLE I. *Experimental treatments.*

Ring No.	Material	Thickness cm (10)$^{-3}$ Stock	Ring	Solution (0.5 N) of	Current density amp. cm^{-2} ×(10)$^{-3}$	Time hr.	Notes
1	CRS	56	56	H_2SO_4	12	0–44	(a) (b)
					24	44–73	(b)
					48	73–121	(b)
2	CRS	56	56	H_2SO_4	12	0–64	(a) (c)
3	CRS	56	56	H_2SO_4	3	0–240	(a) (d)
4	CRS	56	56	KOH	160	0–120	(a)
					400	120–216	
5	CRS	56	56	KOH	1400	0–48	(a) (d)
6	CRS	56	56	H_2SO_4	12	0–96	(e)
7	CRS	216	216	H_2SO_4	12	0–104	(f) (g)
8	CRS	216	216	KOH	12	0–48	(f)
				H_2SO_4	12	48–169	(c) (h)
9	CRS	216	216	H_2SO_4	0	0–200	(f) (i)
10	CRS	317	317	H_2SO_4	12	0–115	(f) (j)
11	CRS	317	317	H_2SO_4	12	0–228	(f)
12	Armco	79	79	H_2SO_4	12	0–203	(a) (k)
					48	203–231	
					3	231–252	
					48	252–324	
13	Armco	79	79	H_2SO_4	48	0–161	(a)
14	Armco	79	79	H_2SO_4	192	0–60	(a)
					0	60–62	
					192	62–120	
15	Armco	79	79	H_2SO_4	6	0–336	(a) (d)
16	Armco	316	316	H_2SO_4	48	0–330	(f) (l)
					192	330–374	
17	CRS	316	56	H_2SO_4	12	0–100	(f) (m) (n)
18	Armco	316	56	H_2SO_4	48	0–208	(f) (m)

(a) Heat treatment: 6 hours at 1500°C in H_2 at atmospheric pressure; cooled in H_2 to 880°C; pumped down to a pressure of the order of 0.1 mm; 2 hours at 880°C; furnace cooled to room temperature.
(b) Electrolysis stopped during magnetic tests. This allowed too much attack by acid so that in all other cases (except in Ring No. 12) the electrolysis was continued at very low current density during magnetic tests.
(c) Magnetic field in ring ($H = 18$) throughout, except as necessarily removed for magnetic testing.
(d) Electrolysis in an open tank (no magnetic tests during progress).
(e) High temperature treatment in hydrogen omitted. Annealed 3 hours at 850°C in vacuum.
(f) Heat treatment: same as (a) except for longer times, 12 hours at 1500°C and 3 hours at 880°C.
(g) Subsequently placed in a toroidal wooden box and wound with primary and secondary. Magnetically tested at intervals for 5 months. See Table III.
(h) Subsequently annealed at various temperatures. See Table IV.
(i) Ring so much attacked by acid that magnetic measurements were no longer possible even with corrections for change in cross section.
(j) Charging current interrupted for an unknown period not exceeding 8 hours.
(k) In dilute HNO_3 one hour before placing in electrolytic cell. Electrolytic current not turned down during magnetic testing. Results of magnetic tests corrected for presence of electrolytic current in a separate experiment.
(l) In dilute H_2SO_4 one hour before placing in electrolytic cell.
(m) Ground down before anneal at 880°C.
(n) Piece fell out of ring, preventing further study of magnetic properties.

EXPERIMENTAL METHODS AND RESULTS

The specimens were rings (6.35 cm outside diameter, 5.08 cm inside diameter) punched or lathe cut from sheets of cold rolled steel (CRS in Table I) or of Armco iron. All rings of a given stock thickness came from a single sheet. The standard treatments before use, Table I, notes (a), (f), should have reduced ordinary impurities to the point where chemical analysis is uninformative, and analysis was therefore not attempted.[10] Magnetic results show that we did not attain maximum possible purity, partly, no doubt, because the hydrogen supplied to our furnace passed over hot alundum before reaching the specimens. All rings were magnetically soft enough, nevertheless, to make even slight hardening easily apparent. We attach no importance to the absolute values of the magnetic constants as reported in Table II and, except as noted in the discussion, data for one ring are to be compared only with earlier or later data for the same ring.

[10] We are indebted to Mr. Cioffi for information regarding his methods and results prior to publication.

TABLE II. *Magnetic properties—electrolysis.*

Ring No.	μ_{max} Before	μ_{max} After	B_r Before	B_r After	H_c Before	H_c After	Rapid change between hrs.
1	23300	8550	13070	5300	0.227	0.332	3–15
2	21400	6720	13800	5690	.267	.418	8–18
3	16300	16300	9230	9230	.182	.182	—
4	14800	14800	13200	13150	.570	.574	—
5	20400	11900	11190	6120	.180	.180	(?)
6	11900	2800	15700	6710	.607	1.20	11–48
7	32400	6240	12140	3840	.135	.230	0–55
8	21900	7750	9800	4400	.151	.257	60–85
9	19000	20300	13500	12100	.243	.225	—
10	35800	15860	10440	4420	.211	.246	16–110
11	29900	13800	12660	4930	.157	.168	92–210
12	25130	12430	10670	5060	.148	.210	96–154
	12430	4720	5060	3070	.210	.391	203–300
13	19300	4600	7410	3320	.138	.380	95–123
14	18000	6080	6280	2610	.170	.255	66–96
15	17100	17000	5820	5790	.151	.150	—
16	15960	2460	4120	1980	.103	.475	155–224
17	15800	15800	8000	8000	.184	.184	—
18	20200	3970	9320	3000	.142	.449	165–195

Fig. 1 shows the electrolytic cell in which rings were charged with hydrogen under conditions described in Table I, and in which magnetic characteristics presented in Table II were obtained. The solution was kept flowing through the cell throughout a test, and loss of water was made good at frequent intervals. Charging current density was generally reduced below (10)$^{-3}$ amp. cm^{-2} during magnetic tests to prevent "cross-talk" between charging and gal-

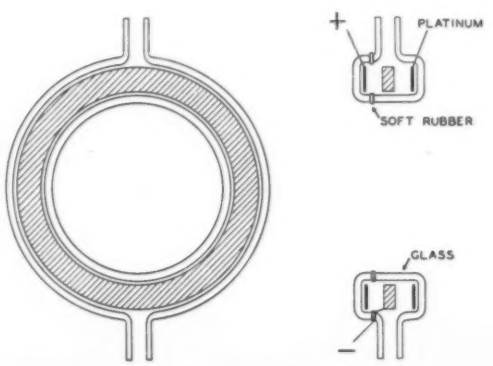

FIG. 1. Electrolytic cell (sections).

TABLE III. *Magnetic properties—aging at room temperature.*

Ring No. 7	μ_{max}	B_r	H_c
Before electrolysis	32400	12140	0.135
0 hr. after electrolysis	6250	3710	.236
14 hr. after electrolysis	6250	3770	.235
40 hr. after electrolysis	6250	3790	.233
13 days after electrolysis	6250	3810	.233
3 months after electrolysis	6240	3840	.231
5 months after electrolysis	6240	3840	.230

TABLE IV. *Magnetic properties—annealing.*

Ring No. 8	μ_{max}	B_r	H_c
Before electrolysis	21900	9800	0.151
After electrolysis	7750	4400	.257
After 17 hr. at 400°C	7800	4400	.256
After 12 hr. at 550°C	9750	6350	.223
After 12 hr. at 830°C	15800	7650	.180

vanometer circuits. The rings fitted the cell so loosely as to prevent strain in assembly or as a result of ordinary temperature changes. Charging from both sides (in a vertical plane) tended to reduce mechanical and magnetic asymmetry. No change in dimensions of as much as one part in 10,000 could be detected in experiments (not reported in Table I) where such changes were looked for.

Magnetic measurements were made by ballistic galvanometer (Leeds and Northrup Type R, sensitivity 0.0003 microcoulomb per scale division). A typical winding (not shown in Fig. 1) might consist of a primary of 300 turns of No. 26 (0.0405 cm) enameled copper wire, with a secondary of 1000 turns of No. 32 (0.0202 cm) enamelled copper wire, both distributed over the whole circumference. Complete magnetization curves and hysteresis loops, usually up to $H_{max}=45$, were taken only at beginning and end of an electrolysis. During a run only enough points were taken to give approximate values of μ_{max}, B_r and H_c at chosen epochs. An effort was made to fix the times at which any important change began and ended. Table II is a condensed account of these major effects.

Figs. 2, 3 and 4 show typical magnetic results. The most striking feature is that even when magnetic properties eventually change most profoundly there may be little or no change for a long time, then a relatively rapid change, and finally another period of constancy. All large and delayed changes of this sort increase magnetic hardness. If there is any immediate effect it is a relatively small decrease in magnetic hardness (Fig. 4).

The results of a few special aging and annealing tests are presented in Tables III and IV.

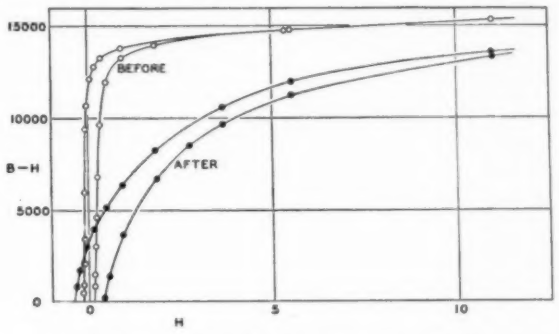

FIG. 3. Hysteresis loops for ring No. 12.

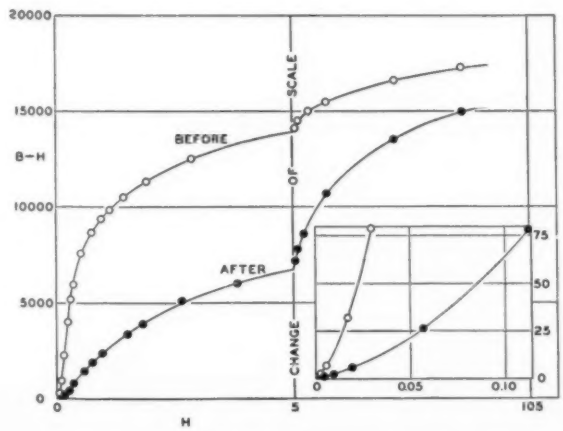

FIG. 2. Magnetization curves for ring No. 16.

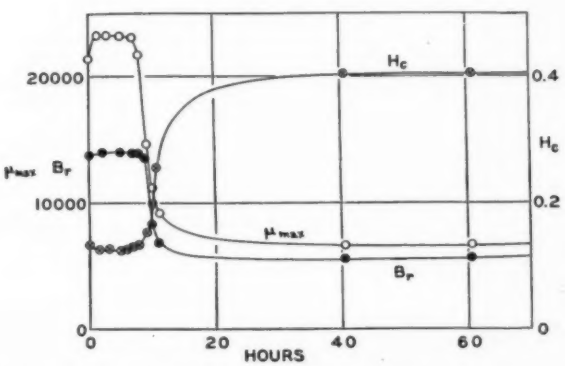

FIG. 4. μ_{max}, B_r, H_c as functions of time of electrolysis for ring No. 2.

Discussion

These experiments and others available for comparison seem consistent with the following simple picture of what happens when hydrogen is liberated at the surface of an iron specimen in an electrolytic cell.

Mere immersion in dilute acid, without any current flowing, relieves surface strains and produces slight magnetic softening. This change is not observed in KOH solutions, is relatively more important in thinner rings, and can be prevented from occurring during electrolysis in H_2SO_4 solutions by preliminary etching with HNO_3, which does not liberate H^+. Small adherent grains of alundum fall off during this initial softening or during any treatment which prevents its occurrence.

Nascent hydrogen enters iron readily at grain boundaries or other crystal imperfections which reach the surface of the piece. Penetration of relatively thick pieces takes but a short time—of the order of one hour or less—results in mechanical brittleness in fine-grained metal,[11] but has almost no magnetic effects. In the present investigation the grains had dimensions of the order of a millimeter or more and embrittlement was not observed.

Hydrogen diffuses more slowly into the more nearly perfect parts of the grains and there is some evidence for the idea that the larger such regions are the longer it takes to saturate the entire specimen with hydrogen, supplied at the same adequate rate in all cases. At least it was observed here that metal of greater purity, as judged by larger grain size and higher corrosion resistance, required a longer time for the onset of profound changes of magnetic behavior. Diffusion of hydrogen in iron is probably atomic rather than molecular, to judge by its dependence on current density.[12] The relatively small effect of thickness upon the time required for saturation (onset of magnetic changes) suggests that the diffusion coefficient increases as saturation is approached. Rings 16 and 18 may be cited in support of this idea. The fact that abrupt magnetic changes still occur with relatively high current density also favors this hypothesis.

If we regard the iron as just saturated with hydrogen when important magnetic changes begin it follows at once that isotropic annealed iron saturated with hydrogen at room temperature is still magnetically soft. Magnetic hardening must then be associated with some sort of "supersaturation." We propose to use this term with some caution, for the easy escape of hydrogen from embrittled iron shows that at least a part of the metal may already be supersaturated at a very early stage of the process. It has been suggested by Alexejew and co-workers[1] that the hydrogen thus loosely bound is concentrated in grain boundaries or in ultramicroscopic cracks. We must conclude, if this is correct, that hydrogen may escape from the free surface of an iron wall before all the grains composing the wall have been supersaturated in the sense here intended.

There seems to be a threshold current density, of the order of $(10)^{-2}$ amp. cm^{-2} in the 0.5N H_2SO_4 here used, below which large magnetic effects are not observed. In KOH solutions at the same normality this threshold is much higher, and it probably depends in both cases upon the purity of the electrolyte, for Alexejew[1] found no embrittlement in H_2SO_4 solutions free from H_2S and other hydride forming impurities. Whether this threshold is exceeded little or much, about the same magnetic hardening finally occurs, the only important differences lying in the time for onset of the change and in the period for its completion. These times are of the order of those apparently necessary for the attainment of stationary conditions in the transport of hydrogen through iron sheets of comparable thicknesses, as in the experiments of Fuller[9] and others.[13]

The magnetic results, when notable change occurs, suggest that the iron has been cold worked. Not only do comparable changes result from over-strain by stretching or rolling, but the low temperature for recovery—below 550°C—is characteristic of plastically deformed iron. We find a plausible process for such cold work in the internal liberation of hydrogen from super-

[11] J. H. Andrew, Trans. Faraday Soc. **9**, 316 (1913); **14**, 232 (1919).

[12] Probably proportional to the square root of current density. See M. Bodenstein, Zeits. f. Elektrochemie **28**, 517 (1922); G. Borelius and S. Lindblom, Ann. d. Physik **82**, 201 (1927).

[13] Most recently commented upon by C. A. Edwards, Nature **133**, 379 (1934).

saturated metal. The threshold current density, on this view, is that necessary to maintain flow through the iron against a back pressure great enough to produce plastic deformation. At a given current density the volume of cold-worked metal rises rather rapidly as soon as the process begins and the process stops as soon as all the metal is strain-hardened. Tests show that the entire volume of the rings is affected and that the condition is unaltered by low temperature processes which remove hydrogen but do not promote recrystallization.

During the cold-working process, at least, the hydrogen is non-uniformly distributed, which explains why so low an average concentration, probably under one atom of hydrogen per hundred atoms of iron,[14] can be effective. The small difference in the time for complete hardening in rings of different thicknesses makes it probable that hydrogen is being fed at once to all points of weakness through many channels of low resistance rather than entering by plane diffusion from the exposed surface. Coulson's experiments[2] on permanent magnet steels show particularly rapid changes.

Cooling iron saturated at a high temperature—in the annealing range or higher—may result in temporary brittleness[15] but no permanent hardening has been detected by either mechanical or magnetic tests.

We must suppose that embrittlement by the initial entry of hydrogen is not accompanied by any cold work of the sort here postulated, for if it were it is hard to see why it should not immediately progress at the expense of soft magnetic material and give a much earlier onset of magnetic hardening. The sharp separation between magnetically ineffective saturation and magnetically effective supersaturation must be insisted upon.

Bridgman[16] has reported premature and progressive deterioration of steel under very high pressures of molecular hydrogen at room temperature. This suggests that the cold work we postulate may occur under any conditions which supersaturate part of the metal, especially if high elastic strains already exist.

Conclusion

Nothing has been said about any effects of magnetic fields superposed during electrolysis (rings 2 and 8), nor about the possible acceleration of magnetic changes by corrosion. These and other points of interest must be left unsettled. It is hoped that this publication will call attention to the imperfections of the theory outlined above, and stimulate its correction or replacement.

The author is indebted to Professor L. W. McKeehan for suggesting this investigation and for help in arranging the results for publication.

[14] R. Chandler, J. Soc. Telegraph Eng. **9**, 168 (1880); M. Thoma, Zeits. f. physik. Chemie **3**, 69 (1889); A. Thiel and W. Hammerschmidt, Zeits. f. anorg. Chemie **132**, 15 (1923); H. O. von Samson-Himmelstjerna, Zeits. f. anorg. Chemie **186**, 337 (1930).

[15] E. Heyn, Stahl u. Eisen **21**, 913 (1901); Metallographist **6**, 39 (1903); H. Jellinek, Zeits. f. Physik **66**, 543 (1930).

[16] P. W. Bridgman, Proc. Am. Acad. **59**, 173 (1924).

The Piezoelectric Properties of Quartz and Tourmaline

GERALD W. FOX AND GEORGE A. FINK, *Physics Laboratory, Iowa State College*

(Received January 23, 1934)

The piezoelectric properties of quartz and tourmaline have been investigated through a study of the converse piezoelectric effect. In the case of quartz, the piezoelectric constant has been measured from point to point across the specimen. Considerable variation in the "constant" has been observed in different samples of quartz. Attention is called to difference between the motions of piezoelectric plates when subjected to static electric fields and when subjected to alternating electric fields.

INTRODUCTION.

IN preparing quartz piezoelectric plates, it frequently occurs that blanks cut from neighboring positions in a crystal of optical quality, even though treated identically in the finishing process, produce oscillators of widely different abilities. Methods are available for locally testing oscillator blanks by applying pressure and observing the resultant charge developed (direct piezoelectric effect) and, although these show that there exists considerable non-uniformity in quartz, they give little information about the absolute value of the piezoelectric constant from point to point. It was, therefore, thought worth while to investigate the local variations in the piezoelectric quality of quartz by using the converse effect wherein an electric field is applied to the plate and the change in thickness measured.

Most previous determinations of piezoelectric constants by the direct effect have necessarily given only the average for the specimen tested since no means was provided for determining how much of the charge liberated came from any particular area of the face.[1, 2, 3] Even a method using concentrated loads, such as that of Dawson,[4] is questionable for evaluating a piezoelectric constant at a point. A contact point with dimensions smaller than the thickness of the plate being tested sets up a very complicated system of stresses and strains. Under these conditions, it seems rather doubtful whether the charge collected by the contact point or probe is simply equal to the product of the applied force and the piezoelectric constant. In the first place, the contact point or probe may not collect all the charge produced if the quartz does not have a conducting coat, since portions of the quartz surface, not in contact with the probe, are strained and produce surface charges. Secondly, the proportionality between strain and polarization may fail when the stress producing them is very high. Thirdly, at many points in the quartz, the stress is not acting along the normal to the surfaces and other constants play a part beside the one appropriate to uniform stress along the normal to the surfaces of the quartz plate.

Even in the present method, elements of the plate are not free to expand independently but are elastically bound together. However, the applied field is uniform. To get a corresponding state of affairs with the direct effect, it would be necessary to apply uniform pressure over the faces of the quartz and measure the charges produced on selected areas of the surface. The only previous determination by the converse effect known to the authors, that of (Ny Tsi)Ze,[5] measured an average value for the specimen. Ze's method gave the interesting result of an apparent saturation with strong fields, but he could only test a long thin piece or a stack of plates.

To test a single piece the size of an oscillator blank by the converse effect, an extremely sensitive method is necessary for measuring the resulting thickness changes. These are only of the order of 10^{-7} cm at an applied potential

[1] J. Curie and P. Curie, J. de physique [2] **1**, 246 (1882).
[2] E. Riecke, and W. Voigt, Ann. d. Physik **45**, 549 (1892).
[3] W. C. Röntgen, and A. Joffe, Ann. d. Physik [4] **41**, 490 (1913).
[4] Dawson, Phys. Rev. **29**, 553 (1927).
[5] Ny Tsi Ze, J. de physique et le radium [6] **9**, Part 1, page 13 (1928).

difference of 500 volts. The amplifying lever developed for these measurements has already been described.[6]

Results

Variation of constant from point to point

This lever and connected apparatus, which might be called a piezoelectric dilatometer, was first set up with three foil-coated plates of glass about two millimeters thick under its three knife edges. No movement of the interference fringes used for observation could be seen when potential differences up to 500 volts were applied to the plates. A movement of one-tenth of a fringe, corresponding to a change in thickness of 0.15A, could have been detected. The fringe shifts observed later with average quartz plates were in the neighborhood of six or seven times the distance between fringes. A quartz plate with faces normal to the optic axis and a piece of fused quartz gave shifts of 1.2 and 1.3 fringes on 500 volts when substituted for the middle glass plate, but this, being the same for both directions of the applied field, was an electrostatic or electrostrictive effect.

Three blanks, numbers 37, 38 and 39, that had been cut with faces normal to the three electric axes of the same crystal, were tested and the positive directions of the axes were found to agree with Fig. 1. The positive direction of an electric axis is the direction of the electric field which produces an expansion of the crystal along the same axis. The piezoelectric deformations were nearly proportional to the applied voltages, as may be seen from the data plotted in Fig. 2. The points are not quite on a straight line; showing that, besides the linear piezoelectric effect, there is an electrostrictive or other effect proportional to the square of the voltage. If the average of two fringe shifts is taken, one with the field equal in strength but opposite in direction, those effects proportional to the square of the voltage will be eliminated. This has been done to obtain the points in Fig. 3 which are seen to lie on a straight line to within the limit of experiment error. The crosses in Figs. 2 and 3 represent readings taken with the center knife edge of the dilatometer resting on a spot near

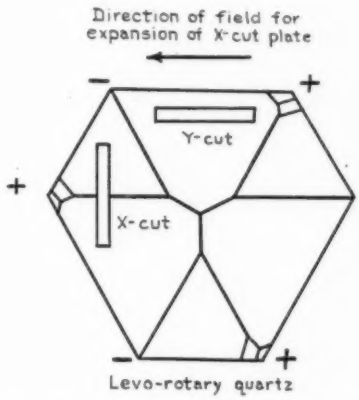

FIG. 1. End view of quartz crystal showing X- and Y-cuts.

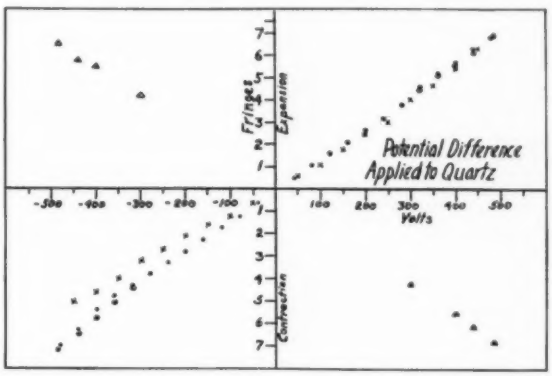

FIG. 2. Data for plate 37 with varying voltage.

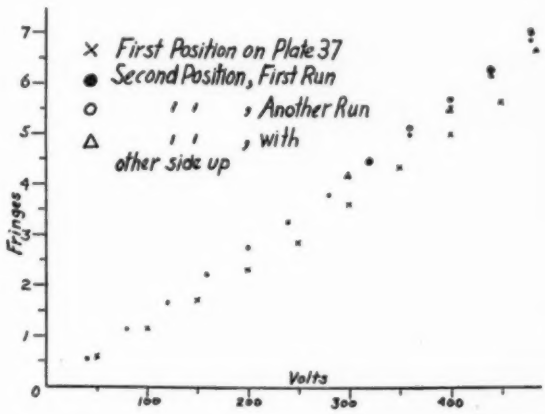

FIG. 3. Data of Fig. 2 averaged for + and − voltages.

the center of plate 37. The plate dimensions were about 12×15×2 mm. The piezoelectric constant, d_{11} in the usual notation,[7] calculated from these data, is 5.17A/e.s.u. With the plate

[6] Fox and Fink, Rev. Sci. Inst. **4**, 276 (1933).

[7] W. G. Cady, Int. Crit. Tab. **6**, 208.

moved a few millimeters so that the knife edge rested on a different part of the plate, readings were obtained giving d_{11} equal to 6.04A/e.s.u. These readings are represented by the dots in Figs. 2 and 3.

The question then arose whether the difference is due to an actual difference in the piezoelectric properties of the quartz at the two points or to changes in the apparatus caused by moving the quartz and readjusting the amplifying lever. To answer this question, another test was made at the point where the value of 6.04A/e.s.u. was obtained. With the dilatometer readjusted after standing idle a day or two, the result was 6.20A/e.s.u. The readings for this run are represented by the circles in Figs. 2 and 3. Next, the specimen was turned over and readjusted again, taking care to have the knife edge resting as nearly as possible on the same part of the specimen. 5.97A/e.s.u. was the constant found this time. The data are plotted with triangles in Figs. 2 and 3. The variation in the three values 6.04, 6.20 and 5.97 is about the limit of experimental error. However, the difference between the average value at the second spot and the value obtained at the first spot is definitely beyond the limit of experimental error. Two other X-cut plates from the same crystal gave the values 6.1 and 5.5A/e.s.u. at one spot on each.

Three Y-cut blanks from the same crystal were tested and the changes in thickness were found to be much smaller than for the X-cut blanks. Values for the piezoelectric constant at one point on each were: 1.4, 1.1 and 2.2A/e.s.u. The constant connecting the applied voltage and the resulting change in thickness in the case of a Y-cut plate is not d_{11} but it is not clear just what it should be. According to the ordinary theory, assuming uniform structure and equal "strengths" of the three axes at every point, the Y-cut plates should undergo pure shear with no change in thickness. The changes in thickness that were found for this type of plate indicate that the three electric axes at a point in a piece of quartz do not have the same strengths. The orientation of the plates with respect to the axes of the crystal was accurate to within a degree. Errors in orientation would then be expected to produce an expansion of the Y-cut plates less than three percent of the expansion of the X-cut plates; i.e., less than 0.3A/e.s.u., which is much less than the values found.

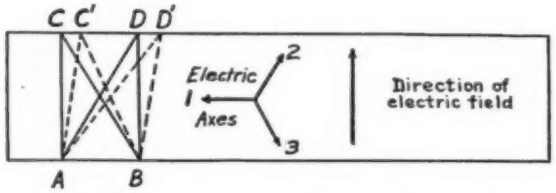

FIG. 4. Deformation of Y-cut plate in an electric field.

A possible explanation on the basis of unequal strengths is illustrated in Fig. 4. The positive directions of the electric axes in a piece of quartz are shown by the arrows 1, 2 and 3. If the field is in the direction shown, it will have no component in the direction of axis 1. It will have a positive component in the direction of axis 2 and will, therefore, cause expansion in that direction. In the direction of axis 3, the field component is negative and, therefore, will produce contraction. If the elongation per unit length in the direction of axis 2 or AD is equal to the contraction per unit length in the direction of BC, then the rectangle $ABDC$ will undergo pure shear and become the parallelogram $ABD'C'$ with no change in altitude, at least to a first approximation. However, if the elongation and contraction per unit length are not equal, the deformation will have some other nature than that of a pure shear and the resulting parallelogram will have an altitude differing from that of the rectangle. It is also possible that some of the apparent changes in thickness of the Y-cut plates—and the X-cut plates, too—may be due to bending of the plates. Bending would be caused by local variations in the expansion along an electric axis and by variations in the corresponding lateral contraction at right angles to this axis.

A specimen of tourmaline 2.39 mm thick was tested next. It was cut with its faces normal to the principal axis which is both the optic and electric axis in this crystal. The piece from which the specimen was cut was roughly triangular in cross section, about 8 mm on a side, green in color except in the center which was yellow. The value of 5.2A/e.s.u. was found at one spot and 5.1A/e.s.u. at approximately the same place with the other side up. The values

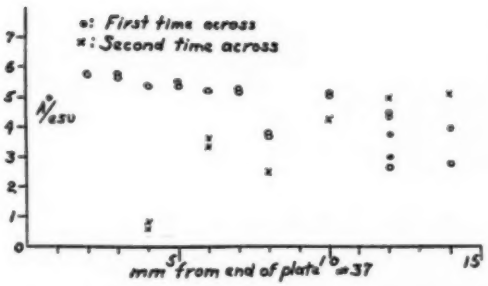

FIG. 5. Variation of the piezoelectric constant across a plate.

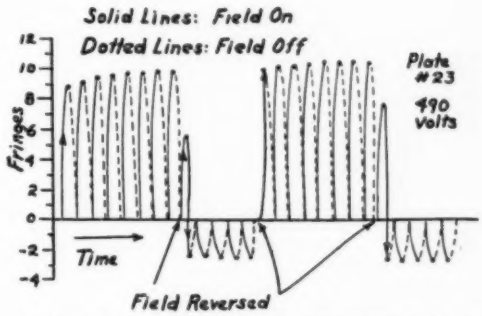

FIG. 6. Showing reversal of fringe movement with reversal of field.

of d_{33} for tourmaline given by Cady[7] are 5.78, 5.4, and 5.6A/e.s.u.

After these first tests indicated that the piezoelectric "constant" varied from point to point across the face of a specimen, the apparatus was changed so that specimens could be moved under the center knife edge without removing the protecting covering and taking the apparatus apart. With this means for moving the specimen, quartz plate number 37 was retested at twelve points approximately a millimeter apart in a line across its face. The results are shown by circles in Fig. 5. Upon going across the face again, testing approximately the same points, the results were quite different as shown by the crosses in Fig. 5. The knife edge which rested on a narrow strip of the specimen's foil coating less than 0.01 mm wide would probably not touch exactly the same spots the second time, but the variations are probably less than $\frac{1}{2}$ mm, certainly much less than 2 mm, the thickness of the plate. It seems unlikely that the change in thickness of a plate 2 mm thick would vary much from one point on its surface to another a half mm away or less, since, to do so, would set up concentrated shearing and bending stresses.

Variation of constants with surface conditions and repeated application of the electric field

The wide discrepancy between the values shown in Fig. 5 for two traverses across the same quartz plate may be due to some of the following causes; different surface conditions, the effects of repeated application of the electric field, possibly changes in the contact between the plate and its support as the plate slides over its support. In any event, further investigations of these peculiar results must be made before an adequate explanation can be offered.

In some further experiments with quartz and glass plates, effects due to repeated application of the electric field were observed. This was especially true of plates that had been coated by cathode sputtering instead of by the original method of coating in which aluminum foil was stuck on with a very small quantity of oil. The movement of the fringes observed upon the first application of the electric field was usually not as great as that attained by repeated application. In one experiment with a glass plate having a sputtered coat, the response when the field was applied the fifteenth time at intervals of about a half minute was nearly three times as great as that obtained the first time. Still more interesting was the behavior when the field was reversed for the first time. The first movement of the fringes, when the field was applied in the reversed direction, was in the same direction as that produced by the original direction of field. This movement would slow down, stop, and reverse, carrying the fringes back to their zero position and beyond to a final steady deflection opposite to that with the original field. The movement out and back to zero took ten or fifteen seconds, while a steady state would be reached in twenty to thirty seconds. When the field was applied again in the second direction, the reversal of movement did not occur, the fringes moving immediately in the direction of the final deflection. Some typical results are shown in Fig. 6. The final "saturated" fringe movements are seen to be fairly consistent.

At some times, a time lag of the fringe movement was observed greater than that due to damping of the motion of the amplifying lever. Records of this lag were made by recording on a chronograph the times of passage of successive

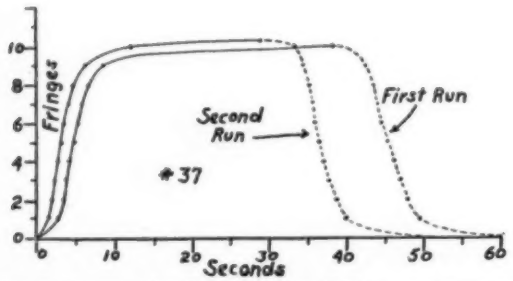

FIG. 7. Curves showing time lag of fringe movements.

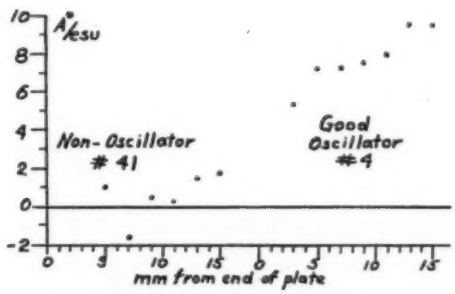

FIG. 8. Comparison of piezoelectric quality of good and poor quartz.

fringes across the intersection of the cross-hairs in the observing telescope. Fig. 7 contains data from two such runs. The slight slope of the flat tops of the curves may be due to leakage currents heating the specimen.

Comparison of an excellent with a worthless blank

The most satisfying results were obtained from a comparison of a specimen from a badly twinned and flawed quartz crystal with a plate that oscillated even though its edges were not carefully ground as is necessary with some inferior blanks. The data plotted in Fig. 8 show that the quartz of poor quality showed a much smaller response at every point than the good quartz, even reversing its sign at one point. The good oscillator gave a large response at every point tested and, except for the lowest point, all are higher than any obtained with any other specimen and higher than the values reported by previous observers using the direct effect.

Remarks on Motions of Plates under Resonance and Static Conditions

It is well to mention that the motions of quartz plates observed in this investigation are not necessarily the ones that the same plates would make in the oscillating circuits where they are customarily used. Though there is no doubt that when a static electric field is applied to an X-cut plate, as was done in this investigation, there is a decided expansion or contraction in the direction of the field, there is considerable doubt that the major surfaces of the plate vibrate as a whole, as is customarily supposed, when the plate is driven at some resonance frequency. The experiments of Osterberg[8, 9, 10, 11] show that the actual motions of quartz plates driven at resonance frequencies are very complex, and are frequently due to coupling between waves reflected from the faces and edges of the plate. The actual motion of the surfaces of a plate is then the resultant of a number of periodic disturbances propagated through the plate. Koga[12] has recently developed a theory which states that the longitudinal thickness vibration is to be expected for the X-cut plates. This has usually been assumed to be the mode of vibration for this type of plate. Interferometer studies, however, have not borne out his idea. The motions of the surfaces of such a plate seem closely dependent upon the shape of the plate and how accurately it has been cut with respect to the faces of the crystal but in no case has actual motion of the major surfaces as a whole been observed except in recent studies by Straubel[13] who states that, by a suitable choice of plate shape, it is possible to produce oscillators having a single resonance frequency in which whole faces vibrate as a unit according to his powder figure studies. According to Koga's theory, the so-called parallel cut always vibrates in the pure shear mode but, here again, interferometer studies do not bear this out.[14] In the static case for the Y-cut, shearing does exist just as expansion along the electric axis exists in the X-cut but it should not be assumed that the motions of a plate under static electric fields are the same as those it would execute if vibrating at a resonance frequency.

[8] H. Osterberg, Proc. Nat. Acad. Sci. **15**, 892 (1929).
[9] H. Osterberg, J. Opt. Soc. Am. **22**, 19 (1932).
[10] H. Osterberg, J. Opt. Soc. Am. **23**, 30 (1932).
[11] H. Osterberg, Phys. Rev. **43**, 819 (1933).
[12] I. Koga, Phil. Mag. (London) **16**, 275 (1933).
[13] Straubel, Phys. Zeits. **32**, 586; **32**, 222 (1931).
[14] Private communications with Dr. Osterberg.

An Inverse Boundary Value Problem in Seismology

CHAIM L. PEKERIS, *Massachusetts Institute of Technology**

(Received May 18, 1934)

It is shown that the variation with depth of the density and elastic constants of a half-space can be determined from the observed motion of the surface caused by a given distribution of stresses on the surface.

INTRODUCTION

THE information one obtains from the interpretation, under the ray concept, of travel-time curves due to a seismic pulse is the variation with depth of the quantities μ/ρ and $(\lambda+2\mu)/\rho$. This method makes use only of the arrival-times of the *P*- and *S*-waves, but not of their form. The question then arises as to what additional information, if any, can be obtained from an analysis of the forms of these waves. Clearly, the relevant observational data are the actual motions of the surface of the earth during the entire passage of the shock, and not the seismogram itself. Let us assume then that from a knowledge of the constants of the seismographs we have reproduced in each case the actual motion of the earth. The resulting record at a given station will depend first of all on the time- and space-variation of the initial pulse. Assuming a definite form for the pulse, we can investigate the resulting motion of the surface when the physical properties of the medium are known. Conversely, if the form of the pulse and the motion of the surface are given, we may attempt to find the physical constants of the medium. We should expect that such an analysis would yield at least the information obtainable from the arrival-times alone.

The problem at hand may be called, in Slichter's terminology, an inverse boundary value problem in elasticity. Similar inverse boundary value problems in electrostatics and electrodynamics have recently been treated by Slichter,[1] Langer[2] and Stevenson.[3] In the following we shall discuss the general features of the forced vibrations of an heterogeneous elastic half-space and shall give a formal solution of the inverse problem for two relevant types of stresses applied at the surface. In the first case the dilatation is zero throughout and the analysis yields the density ρ and the elastic constant μ as functions of depth. In the second case the dilatation is finite and we obtain ρ, μ and the elastic constant λ as functions of depth.

1. STATEMENT OF THE PROBLEM

On the surface of a half-space whose elastic constants λ *and* μ *and density* ρ *vary only with depth is applied a given distribution of stresses; the functions* λ, μ *and* ρ *are to be determined from the observed motion of the surface.* Let the axis of z point downward; then λ, μ and ρ are functions of z only. The general equations of elastic motion in an heterogeneous solid:

$$\rho\frac{\partial^2 u}{\partial t^2}=\frac{\partial}{\partial x}\left(\lambda\delta+2\mu\frac{\partial u}{\partial x}\right)+\frac{\partial}{\partial y}\left[\mu\left(\frac{\partial v}{\partial x}+\frac{\partial u}{\partial y}\right)\right]+\frac{\partial}{\partial z}\left[\mu\left(\frac{\partial w}{\partial x}+\frac{\partial u}{\partial z}\right)\right], \quad (1.1)$$

$$\rho\frac{\partial^2 v}{\partial t^2}=\frac{\partial}{\partial y}\left(\lambda\delta+2\mu\frac{\partial v}{\partial y}\right)+\frac{\partial}{\partial x}\left[\mu\left(\frac{\partial u}{\partial y}+\frac{\partial v}{\partial x}\right)\right]+\frac{\partial}{\partial z}\left[\mu\left(\frac{\partial w}{\partial y}+\frac{\partial v}{\partial z}\right)\right], \quad (1.2)$$

$$\rho\frac{\partial^2 w}{\partial t^2}=\frac{\partial}{\partial z}\left(\lambda\delta+2\mu\frac{\partial w}{\partial z}\right)+\frac{\partial}{\partial x}\left[\mu\left(\frac{\partial u}{\partial z}+\frac{\partial w}{\partial x}\right)\right]+\frac{\partial}{\partial y}\left[\mu\left(\frac{\partial v}{\partial z}+\frac{\partial w}{\partial y}\right)\right], \quad (1.3)$$

with

$$\delta\equiv\partial u/\partial x+\partial v/\partial y+\partial w/\partial z, \quad (1.4)$$

reduce under these assumptions to

* Read at the 1934 Spring meeting of the Eastern Section of the American Seismological Society.

[1] L. B. Slichter, Physics **3**, 273 (1932); **4**, 411 (1933).

[2] R. E. Langer, Bull. Am. Math. Soc. **39**, 184 (1933).

[3] A. F. Stevenson, Physics **5**, 114 (1934).

$$\rho\frac{\partial^2 u}{\partial t^2}=(\lambda+\mu)\frac{\partial\delta}{\partial x}+\mu\nabla^2 u+\frac{d\mu}{dz}\left(\frac{\partial u}{\partial z}+\frac{\partial w}{\partial x}\right), \quad (1.5)$$

$$\rho\frac{\partial^2 v}{\partial t^2}=(\lambda+\mu)\frac{\partial\delta}{\partial y}+\mu\nabla^2 v+\frac{d\mu}{dz}\left(\frac{\partial v}{\partial z}+\frac{\partial w}{\partial y}\right), \quad (1.6)$$

$$\rho\frac{\partial^2 w}{\partial t^2}=(\lambda+\mu)\frac{\partial\delta}{\partial z}+\mu\nabla^2 w+\delta\frac{d\lambda}{dz}+2\frac{d\mu}{dz}\frac{\partial w}{\partial z}. \quad (1.7)$$

Now assume that

$$u\equiv\partial F/\partial x+\partial G/\partial y, \qquad v\equiv\partial F/\partial y-\partial G/\partial x, \qquad w\equiv\partial F/\partial z+w', \quad (1.8)$$

where F, G, and w' are functions of x, y, z and t. We have merely effected here a linear transformation of the variables u, v and w into the variables F, G and w'. On substituting (1.8) in (1.5), (1.6) and (1.7) it is found that the resulting equations are satisfied by the following system of equations:

$$\rho\frac{\partial^2 G}{\partial t^2}=\mu\nabla^2 G+\frac{d\mu}{dz}\frac{\partial G}{\partial z}, \quad (1.9)$$

$$\rho\frac{\partial^2 F}{\partial t^2}=(\lambda+2\mu)\nabla^2 F+(\lambda+\mu)\frac{\partial w}{\partial z}+\frac{d\mu}{dz}\left(2\frac{\partial F}{\partial z}+w'\right), \quad (1.10)$$

$$\rho\frac{\partial^2}{\partial t^2}\left(\frac{\partial F}{\partial z}+w'\right)=(\lambda+\mu)\left(\frac{\partial\nabla^2 F}{\partial z}+\frac{\partial^2 w'}{\partial z^2}\right)+\mu\left(\frac{\partial\nabla^2 F}{\partial z}+\nabla^2 w'\right)+\frac{d\lambda}{dz}\left(\nabla^2 F+\frac{\partial w'}{\partial z}\right)+2\frac{d\mu}{dz}\left(\frac{\partial^2 F}{\partial z^2}+\frac{\partial w'}{\partial z}\right). \quad (1.11)$$

The boundary conditions are that the functions shall be bounded (except, perhaps, at points of discontinuity of the applied stresses) and that the stresses

$$p_{zz}=\lambda\delta+2\mu\partial w/\partial z, \quad (1.12)$$

$$p_{xz}=\mu(\partial w/\partial x+\partial u/\partial z), \quad (1.13)$$

$$p_{zy}=\mu(\partial w/\partial y+\partial v/\partial z) \quad (1.14)$$

at the surface ($z=0$) shall equal the prescribed *applied* stresses. Noticing that

$$\delta=\nabla^2 F+\partial w'/\partial z \quad (1.15)$$

it is clear from the above equations that also in a heterogeneous medium two types of elastic motion are possible:[4] one without dilatation corresponding to

$$G\neq 0, \qquad F\equiv 0, \qquad w'\equiv 0, \quad (1.16)$$

and one with dilatation corresponding to

$$G\equiv 0, \qquad F\neq 0, \qquad w'\neq 0. \quad (1.17)$$

Moreover, in the first case the motion is purely horizontal and the normal stress p_{zz} is everywhere zero, while in the second case the vertical component of the curl of the displacement is everywhere zero.

2. Case of a Non-Dilatational Disturbance

Let us begin with a discussion of the solutions of (1.9) which are periodic in time:

$$G(x, y, z, t)=e^{ipt}H(x, y, z). \quad (2.1)$$

In a cylindrical system of coordinates, equation (1.9) becomes

$$\mu\left(\frac{\partial^2 H}{\partial r^2}+\frac{1}{r}\frac{\partial H}{\partial r}+\frac{1}{r^2}\cdot\frac{\partial^2 H}{\partial\theta^2}+\frac{\partial^2 H}{\partial z^2}\right)+\frac{d\mu}{dz}\frac{\partial H}{\partial z}+p^2\rho H=0. \quad (2.2)$$

The radial and azymuthal displacements, which we shall denote by u and v, respectively, are according to (1.8) given by

$$u=(1/r)\partial G/\partial\theta, \qquad v=-\partial G/\partial r; \quad (2.3)$$

the corresponding stresses are seen to be

$$p_{zr}=\mu(\partial u/\partial z), \quad (2.4) \qquad p_{z\theta}=\mu(\partial v/\partial z). \quad (2.5)$$

We shall limit ourselves to solutions which are symmetrical about the z-axis. Thus:

$$u=p_{zr}=0. \quad (2.6)$$

Under this assumption Eq. (2.2) is satisfied by

$$H(r, z)=R(r)\cdot Z(z)$$

and

$$\frac{d^2R}{dr^2}+\frac{1}{r}\frac{dR}{dr}+k^2R=0, \quad (2.7)$$

[4] This result was given first by J. H. Jeans, Proc. Roy. Soc. **A102**, 554 (1923).

$$\frac{d^2Z}{dz^2}+\frac{1}{\mu}\frac{d\mu}{dz}\frac{dZ}{dz}-(k^2-p^2\rho/\mu)Z=0. \qquad (2.8)$$

An appropriate solution of (2.7) is the Bessel function $J_0(kr)$. Of the solutions of (2.8), we adopt the one which for a fixed value of p and $z(\neq 0)$ is asymptotically like e^{-kz} for large values of k, and call it $Z_1(z)$. It follows now from (2.3) that

$$v=kJ_1(kr)Z_1(z)e^{ipt}. \qquad (2.9)$$

Let us seek solutions for v of the form

$$v(z, r, t)=\int_{-\infty}^{\infty}e^{ipt}dp\int_0^{\infty}\varphi(p, k)kJ_1(kr)Z_1(z, k, p)dk. \qquad (2.10)$$

The function $\varphi(p, k)$ has to be chosen so that

$$(p_{z\vartheta})_{z=0}=\mu_0\int_{-\infty}^{\infty}e^{ipt}dp\int_0^{\infty}\varphi(p, k)kJ_1(kr)\dot{Z}_1(0, k, p)dk=f(r, t), \qquad (2.11)$$

$f(r, t)$ being the stress applied at the surface. The quantity that is observed is

$$v(0, r, t)=\int_{-\infty}^{\infty}e^{ipt}dp\int_0^{\infty}\varphi(p, k)kJ_1(kr)Z_1(0, k, p)dk. \qquad (2.12)$$

Now the integrals in (2.11) and (2.12) are of the type which can be inverted by an application of the Fourier identity:

$$F(t)\equiv(1/2\pi)\int_{-\infty}^{\infty}e^{ipt}dp\int_{-\infty}^{\infty}F(\lambda)e^{-ip\lambda}d\lambda, \qquad (2.13)$$

and the Fourier-Bessel identity:

$$F(r)\equiv\int_0^{\infty}J_v(kr)kdk\int_0^{\infty}F(R)J_v(kR)RdR, \qquad (2.14)$$

provided that $\int_{-\infty}^{\infty}|F(t)|dt$ and $\int_0^{\infty}F(r)(r)^{\frac{1}{2}}dr$ exist and are absolutely convergent. We can therefore write formally

$$\varphi(p, k)Z_1(0, k, p)=(1/2\pi)\int_0^{\infty}J_1(kr)rdr\int_{-\infty}^{\infty}v(0, r, t)e^{-ipt}dt, \qquad (2.15)$$

$$\varphi(p, k)\dot{Z}_1(0, k, p)=(1/2\pi\mu_0)\int_0^{\infty}J_1(kr)rdr\int_{-\infty}^{\infty}f(r, t)e^{-ipt}dt. \qquad (2.16)$$

The inversion of (2.11) can certainly be justified for the type of stresses that are likely to occur, since the stresses will be finite everywhere and will vanish beyond certain values of r and of t. With $\varphi(p, k)$ thus defined by (2.16), the question arises as to the types of media for which (2.12) converges and the subsequent inversion permissible. We shall not enter here upon a discussion of this question, and shall assume the convergence of the integrals involved.[5] Equations (2.15) and (2.16) determine $\dot{Z}_1(0, k, p)/Z_1(0, k, p)$ as a function of the parameters k and p. It is from this quantity, taken in conjunction with the defining Eq. (2.8), that we wish to determine $\rho(z)$ and $\mu(z)$.

[5] The question of convergence of the integrals appearing in this and the following sections is bound up with the problem of free vibrations of the medium and with the condition that (2.10), (3.10) and (3.11) shall represent diverging waves.

Following Langer, let us investigate the asymptotic behavior of Z_1 for large values of k. With $Z \equiv e^{\int^z U(z)dz}$, Eq. (2.8) becomes

$$\dot{U}+U^2+(\dot{\mu}/\mu)U+p^2(\rho/\mu)-k^2=0. \quad (2.17)$$

Assume

$$U \equiv \dot{Z}/Z = kU_1+U_0+(1/k)U_{-1} +(1/k)^2U_{-2}\cdots,^6 \quad (2.18)$$

substitute in (2.17) and equate the coefficients of each power of k to zero. The coefficient of k^2 is (U_1^2-1), the root of interest to us being $U_1=-1$. With this value for U_1 the other equations are:

$$\dot{\mu}/\mu=-2U_0, \quad (2.19)$$

$$\dot{U}_0-2U_{-1}-U_0^2+p^2(\rho/\mu)=0, \quad (2.20)$$

$$\dot{U}_{-1}-2U_{-2}=0, \quad (2.21)$$

$$\dot{U}_{-2}-2U_{-3}+U_{-1}^2=0, \quad \text{etc.} \quad (2.22)$$

If we now develop $[k+\dot{Z}_1(0, k, p)/Z_1(0, k, p)]$ into a descending power series in k, we can identify the various coefficients with the corresponding U's in (2.18). The U's are, in general, functions of the parameter p^2. We can see, however, from (2.19) that U_0 is independent of p^2, since it equals a function of z only. It follows from (2.20) that

$$U_{-1}=U_{-10}+p^2U_{-11}, \quad (2.23)$$

and that

$$\dot{U}_0-2U_{-10}-U_0^2=0, \quad (2.24) \qquad 2U_{-11}=\rho/\mu. \quad (2.25)$$

From (2.21) we now infer that

$$U_{-2}=U_{-20}+p^2U_{-21}, \quad (2.26)$$

$$\dot{U}_{-10}-2U_{-20}=0, \quad (2.27)$$

$$\dot{U}_{-11}-2U_{-21}=0. \quad (2.28)$$

Similarly we infer from (2.22) that

$$U_{-3}=U_{-30}+p^2U_{-31}+p^4U_{-32}, \quad (2.29)$$

$$\dot{U}_{-20}-2U_{-30}+U_{-10}^2=0, \quad (2.30)$$

$$\dot{U}_{-21}-2U_{-31}+2U_{-10}\cdot U_{-11}=0, \quad (2.31)$$

$$2U_{-32}=U_{-11}^2, \quad \text{etc.} \quad (2.32)$$

Turning now to (2.19), we see that it determines $(\dot{\mu}/\mu)$ for $z=0$. When this equation is differentiated, it yields in conjunction with (2.24) $d/dz(\dot{\mu}/\mu)$ at $z=0$. Similarly, one can obtain the higher derivatives of $(\dot{\mu}/\mu)$ from (2.27), (2.30), etc., each taken in conjunction with the derivatives of the preceding equations. In the same manner (2.28) determines $d/dz(\rho/\mu)_0$, (2.31) and (2.28) once differentiated determine $d^2/dz^2(\rho/\mu)_0$, etc. In this way we can obtain a power series development of μ and ρ at the origin.

It should be noticed that μ_0 has to be determined by an examination of the surface material, while $(\rho/\mu)_0$ is given by (2.25); also that we make use only of the equations starting with either $\dot{U}_{-k0}$, or $\dot{U}_{-k1}$. Of the other equations, those which begin with $\dot{U}_{-kn}(n>1)$ are irrelevant, while an equation of the type (2.32) imposes a relationship between observable quantities. This feature is, however, a direct consequence of the differential equation in much the same way as the fact that the asymptotic development of $\dot{Z}_1(0, k, p)/Z_1(0, k, p)$ for large values of k starts with the term $(-k)$.

If the applied stress, instead of being an arbitrary function of the time, were of a definite frequency p, the resulting motion would be periodic and of the same frequency. The coefficients U_k in (2.18) would no longer be functions of the parameter p^2 and the only result of the analysis would be a power series expansion for $\mu(z)$. The arbitrariness of the variation in time of the applied stress, which amounts to a simultaneous application of pulses of all frequencies, is then the circumstance which makes possible the determination of $\rho(z)$.

To sum up, we have shown that when a radially symmetrical twisting stress is applied at the surface of a heterogeneous medium, the functions $\rho(z)$ and $\mu(z)$ can be determined uniquely from the observed surface motion by a process which involves only the operations of integration and the expansion in a power series.

[6] The asymptotic solutions of (2.8) for large values of p are $e^{\pm ip\int^z(\rho/\mu)^{\frac{1}{2}}dz}$. These correspond to the solutions under the ray-concept, since, by (2.1), they represent waves travelling with a velocity $(\mu/\rho)^{\frac{1}{2}}$.

3. Case of a Dilatational Disturbance

Let us start out with a discussion of the formal solution of the inverse problem for the case when a radially symmetrical normal stress (p_{zz}) is applied at the surface. The dilatation now being different from zero, the motion will depend on ρ, μ and λ. One would expect therefore that an analysis of the resulting motion would yield all these three functions.

In a cylindrical system of coordinates the radial, azimuthal and vertical displacements are by (1.8)

$$u=\partial F/\partial r, \qquad v=(1/r)\partial F/\partial\theta, \qquad w=\partial F/\partial z+w'. \tag{3.1}$$

If we limit ourselves again to solutions with cylindrical symmetry, we shall have

$$v=\partial F/\partial\theta=p_{z\theta}=0. \tag{3.2}$$

Consider first periodic solutions of (1.10) and (1.11):

$$F(z, r, t)=e^{ipt}R(r)f(z), \qquad w'(z, r, t)=e^{ipt}Q(r)\varphi(z). \tag{3.3}$$

Substitute in (1.10), drop the time factor and divide by $R(r)f(z)$, obtaining after a rearrangement of terms

$$[p^2\rho+(\lambda+2\mu)(\ddot{f}/f)+2\dot{\mu}\dot{f}/f]+(\lambda+2\mu)[\ddot{R}/R+(1/r)\dot{R}/R]+[(\lambda+\mu)(\dot{\varphi}/f)+\dot{\mu}\varphi/f]Q/R=0. \tag{3.4}$$

The dots stand for differentiation with respect to the independent variable in question. Denoting the terms in the first and last brackets of (3.4), respectively, by $u(z)$ and $v(z)$, we have

$$u(z)/v(z)=-[\ddot{R}/R+(1/r)\dot{R}/R](\lambda+2\mu)/v(z)-Q/R. \tag{3.5}$$

Upon differentiating now (3.5) with respect to z and dividing the result by $d/dz[(\lambda+2\mu)/v(z)]$, one obtains an equation one side of which is a function of z only and the other side a function of r only. It follows that

$$\ddot{R}/R+(1/r)\dot{R}/R=-k^2, \qquad \therefore \quad R=J_0(kr). \tag{3.6}$$

Substituting this result into (3.4) we find that Q/R must be a constant, which we take to be unity, since we can absorb any constant factor in $\varphi(z)$ of (3.3). Thus

$$Q(r)=J_0(kr). \tag{3.7}$$

With (3.6) and (3.7), Eqs. (1.10) and (1.11) become, after dropping the common factors,

$$p^2\rho f+(\lambda+2\mu)(\ddot{f}-k^2f)+(\lambda+\mu)\dot{\varphi}+\dot{\mu}(2\dot{f}+\varphi)=0, \tag{3.8}$$

$$p^2\rho(\dot{f}+\varphi)+(\lambda+2\mu)(\dddot{f}-k^2\dot{f}+\ddot{\varphi})-k^2\mu\varphi+\dot{\lambda}(\ddot{f}-k^2f+\dot{\varphi})+2\dot{\mu}(\ddot{f}+\dot{\varphi})=0. \tag{3.9}$$

Upon eliminating one of the variables, one obtains a differential equation of the fourth order in the other variable. We shall, however, later find that when seeking the asymptotic solutions for large values of k the laborious process of elimination can be avoided; also that there exist such solutions which for fixed values of p and $z(\neq 0)$ are like e^{-kz}. Let these elementary solutions be denoted by $f(z)$ and $\varphi(z)$ without subscripts. We now seek solutions for F and w' of the type

$$F(z, r, t)=\int_{-\infty}^{\infty}e^{ipt}dp\int_0^{\infty}N(p, k)J_0(kr)f(z, k, p)dk,$$

$$w'(z, r, t)=\int_{-\infty}^{\infty}e^{ipt}dp\int_0^{\infty}N(p, k)J_0(kr)\varphi(z, k, p)dk.$$

Hence
$$u\equiv\partial F/\partial r=-\int_{-\infty}^{\infty}e^{ipt}dp\int_0^{\infty}N(p,k)kJ_1(kr)f(z,k,p)dk, \tag{3.10}$$

$$w\equiv\partial F/\partial z+w'=\int_{-\infty}^{\infty}e^{ipt}dp\int_0^{\infty}N(p,k)J_0(kr)[\dot f(z,k,p)+\varphi(z,k,p)]dk, \tag{3.11}$$

$$\delta\equiv\nabla^2F+\partial w'/\partial z=\int_{-\infty}^{\infty}e^{ipt}dp\int_0^{\infty}N(p,k)J_0(kr)[\ddot f-k^2f+\dot\varphi]dk, \tag{3.12}$$

$$p_{zz}\equiv\lambda\delta+2\mu\partial w/\partial z=\int_{-\infty}^{\infty}e^{ipt}dp\int_0^{\infty}N(p,k)J_0(kr)[(\lambda+2\mu)(\ddot f+\dot\varphi)-\lambda k^2f]dk, \tag{3.13}$$

$$p_{zr}\equiv\mu[(\partial w/\partial r)+(\partial u/\partial z)]=-\mu\int_{-\infty}^{\infty}e^{ipt}dp\int_0^{\infty}N(p,k)kJ_1(kr)(2\dot f+\varphi)dk. \tag{3.14}$$

The vanishing of p_{zr} everywhere on the surface requires[7] that

$$(2\dot f+\varphi)_0=0. \tag{3.15}$$

The function $N(p,k)$ has to be chosen so that (3.13), taken for $z=0$, shall equal $P(r,t)$ – the applied stress. If, as is likely to happen in an actual case, $P(r,t)$ is bounded and vanishes beyond certain values of r and of t, we can invert (3.13) obtaining

$$[(\lambda+2\mu)(\ddot f+\dot\varphi)-\lambda k^2f]_0N(p,k)/k=(1/2\pi)\int_0^{\infty}J_0(kr)rdr\int_{-\infty}^{\infty}P(r,t)e^{-ipt}dt, \tag{3.16}$$

which defines $N(p,k)$. Assuming now the convergence of (3.10) and (3.11) and that they can be inverted for the value $z=0$, we shall have

$$f(0,k,p)N(p,k)=-(1/2\pi)\int_0^{\infty}J_1(kr)rdr\int_{-\infty}^{\infty}u(0,r,t)e^{-ipt}dt, \tag{3.17}$$

$$[\dot f(0,k,p)+\varphi(0,k,p)]N(p,k)/k=(1/2\pi)\int_0^{\infty}J_0(kr)rdr\int_{-\infty}^{\infty}w(0,r,t)e^{-ipt}dt. \tag{3.18}$$

The last three equations determine uniquely

$$[(\dot f+\varphi)/f]_0\quad\text{and}\quad[(\ddot f+\dot\varphi)/f]_0 \tag{3.19}$$

as functions of the parameters p and k.

We are now confronted with a task similar to that of section 2, namely, to determine $\rho(z)$, $\mu(z)$ and $\lambda(z)$ from the two functions in (3.19). For that purpose we must find the asymptotic solutions of (3.8) and (3.9) for large values of k. As a first step let us prove that there exist solutions of the form e^{-kz}. Write $\psi\equiv\varphi+\dot f$, ψ being the elementary z-factor for w. Substitute in (3.8) and (3.9), divide by μ and call

$$p^2\rho/\mu\equiv\alpha,\quad\dot\mu/\mu\equiv\beta,\quad\lambda/\mu\equiv\gamma, \tag{3.20}$$

obtaining
$$\alpha f+\ddot f-k^2(\gamma+2)f+(1+\gamma)\dot\psi+\beta(\psi+\dot f)=0, \tag{3.21}$$

$$\alpha\psi+(\gamma+2)\ddot\psi-k^2(\gamma+1)\dot f-k^2\psi+(\dot\gamma+\gamma\beta)(\dot\psi-k^2f)+2\beta\dot\psi=0. \tag{3.22}$$

[7] See Eq. (3.47).

Further let $$f \equiv e^{\int^z U(z)\,dz}, \quad \psi \equiv e^{\int^z S(z)\,dz}, \quad \therefore \quad d/dz(\psi/f) = (S-U)(\psi/f). \tag{3.23}$$

Substitute in (3.21) and (3.22), divide by f and differentiate once the first equation thus obtained. From the resulting three equations (ψ/f) can be eliminated. One thus obtains two equations in U and S and their derivatives up to the second. If we now assume for U the development (2.18) and a similar development for S, we shall find that the coefficients of (k^4) in the above equations, when set to equal zero, yield the relations:

$$[U_1^2-(\gamma+2)][(\gamma+2)S_1^2-1] = -U_1S_1(\gamma+1)^2, \tag{3.24}$$

$$[U_1^2-(\gamma+2)][(\gamma+1)(S_1^2-U_1S_1)] = 0, \tag{3.25}$$

of which the non-trivial solutions are $U_1 = S_1$ and $U_1 = \pm 1$. We are interested, of course, in the pair $U_1 = -1$, $S_1 = -1$. It follows that, with $\psi \equiv -kg$, we are justified in writing

$$f(z) = e^{-kz}U(z), \qquad g(z) = e^{-kz}S(z), \tag{3.26}$$

$$U(z) = U_0(z)+(1/k)U_{-1}(z)+\cdots, \qquad S(z) = S_0(z)+(1/k)S_{-1}(z)+\cdots. \tag{3.27}$$

The form (3.26) is essentially the same as (3.23), but the functions U and S are not identical with the previously defined functions. By (3.26), Eqs. (3.21) and the difference between (3.21) and (3.22) become

$$\alpha U+\ddot{U}+\beta\dot{U}+k[-2\dot{U}-(\gamma+1)\dot{S}-\beta(U+S)]+k^2(\gamma+1)(S-U) = 0, \tag{3.28}$$

$$\alpha(U-S)+\ddot{U}-(\gamma+2)\ddot{S}+\beta\dot{U}-(\dot{\gamma}+\gamma\beta+2\beta)\dot{S}+k[(\gamma+3)(\dot{S}-\dot{U})+(\dot{\gamma}+\gamma\beta+\beta)(S-U)] = 0. \tag{3.29}$$

On putting the coefficients of the powers of k equal to zero, there result the relations

$$U_0 = S_0,$$

$$(\gamma+1)(S_{-1}-U_{-1})-(\gamma+3)\dot{U}_0-2\beta U_0 = 0, \tag{3.30}$$

$$(\gamma+3)(\dot{S}_{-1}-\dot{U}_{-1})+(\dot{\gamma}+\gamma\beta+\beta)(S_{-1}-U_{-1})-(\gamma+1)\ddot{U}_0-(\dot{\gamma}+\gamma\beta+\beta)\dot{U}_0 = 0, \tag{3.31}$$

$$(\gamma+1)(S_{-2}-U_{-2})-2\dot{U}_{-1}-(\gamma+1)\dot{S}_{-1}-\beta(U_{-1}+S_{-1})+\alpha U_0+\ddot{U}_0+\beta\dot{U}_0 = 0, \tag{3.32}_{0,1}$$

$$(\gamma+3)(\dot{S}_{-2}-\dot{U}_{-2})+(\dot{\gamma}+\gamma\beta+\beta)(S_{-2}-U_{-2})+\alpha(U_{-1}-S_{-1})+\ddot{U}_{-1}-(\gamma+2)\ddot{S}_{-1}+\beta\dot{U}_{-1}$$
$$-(\dot{\gamma}+\gamma\beta+2\beta)\dot{S}_{-1} = 0, \tag{3.33}_{0,1}$$

$$(\gamma+1)(S_{-3}-U_{-3})-2\dot{U}_{-2}-(\gamma+1)\dot{S}_{-2}-\beta(U_{-2}+S_{-2})+\alpha U_{-1}+\ddot{U}_{-1}+\beta\dot{U}_{-1} = 0, \tag{3.34}_{0,1,2}$$

$$(\gamma+3)(\dot{S}_{-3}-\dot{U}_{-3})+(\dot{\gamma}+\gamma\beta+\beta)(S_{-3}-U_{-3})+\alpha(U_{-2}-S_{-2})+\ddot{U}_{-2}-(\gamma+2)\ddot{S}_{-2}+\beta\dot{U}_{-2}$$
$$-(\dot{\gamma}+\gamma\beta+2\beta)\dot{S}_{-2} = 0, \quad \text{etc.} \tag{3.35}_{0,1,2}$$

The values of these functions at $z=0$ are restricted by (3.15), which is equivalent to

$$k(U+S) = \dot{U}. \tag{3.36}$$

Hence we have for $z=0$

$$U_0=S_0=0 \qquad (3.37); \qquad U_{-1}+S_{-1}=\dot{U}_0 \qquad (3.38);$$

$$U_{-2}+S_{-2}=\dot{U}_{-1} \quad (3.39)_{0,1}; \qquad U_{-3}+S_{-3}=\dot{U}_{-2}, \text{ etc.} \quad (3.40)_{0,1,2}$$

The U_{-i} and S_{-i} are in general functions of the parameter (p^2), since α occurs in the defining differential Eqs. (3.30) to (3.35). We can prove, however, that

$$U_{-i}=U_{-i0}+(p^2)U_{-i1}+\cdots+(p^2)^iU_{-ii} \tag{3.41}$$

and similarly for the S_{-i}; also that the values of U_{-i} and S_{-i} at $z=0$ are polynomials of degree $(i-1)$ in (p^2).

We notice first that $(\dot{S}_{-1}-\dot{U}_{-1})$ and $(S_{-1}-U_{-1})$ in (3.31) can be eliminated with the aid of (3.30). There results an homogeneous second-order differential equation for U_0 *with coefficients which are independent of* α. Hence U_0 is independent of p^2. Turning now to (3.33), we see that we can substitute for $(\dot{S}_{-2}-\dot{U}_{-2})$ and $(S_{-2}-U_{-2})$ from (3.32). Also $(U_{-1}-S_{-1})$, $\ddot{S}_{-1}$, and $\dot{S}_{-1}$ can be expressed in terms of U_{-1} and U_0 by (3.30). One thus obtains an inhomogeneous second order differential equation for U_{-1} with coefficients which are independent of p^2 and with a right-hand side which is *linear* in p^2. Since the general solution of an inhomogeneous differential equation is *linear* in the term on the right-hand side, it follows that $U_{-1}=U_{-10}+p^2U_{-11}$. By (3.30) this result holds also for S_{-1}. Similarly one can obtain from (3.35) and the preceding equations an inhomogeneous second order differential equation for U_{-2} with coefficients which are independent of p^2, but with a right-hand side which is quadratic in p^2. In general, the differential equation for U_{-n} or S_{-n} will be inhomogeneous and of the second order; p^2 will occur only on the right-hand side and to the power of n. Hence (3.41) is true.

The initial values of U_{-ii} and S_{-ii} will be zero.[8] This can be established for U_{-11} and S_{-11} from the Eqs. (3.38) and (3.30), the latter taken for $z=0$. One can solve for U_{-1} and S_{-1} in terms of U_0 and hence they cannot contain any (p^2) term. Similar results for U_{-22} and S_{-22} can be established from (3.39) and (3.32), and so on for the other functions. An equation like (3.32), taken for $z=0$, therefore stands for two equations, one independent of (p^2) and the other multiplying (p^2). This multiplicity is designated by the subscripts.

It has been shown previously that it is possible to determine $[(\dot{f}+\varphi)/f]_0$ and $[(\ddot{f}+\dot{\varphi})/f]_0$ as functions of k and p. When taken in conjunction with (3.15) these determine uniquely $(\dot{f}/f)$ and $(\dot{g}/g)$, which in turn determine $\dot{U}/U$ and $\dot{S}/S$. Remembering that $U_0=S_0=0$, we have

$$\dot{U}/U=[\dot{U}_0+(1/k)\dot{U}_{-1}+\cdots]/[(1/k)U_{-1}+(1/k)^2U_{-2}+\cdots]\equiv kL_1+L_0+(1/k)L_{-1}+\cdots, \tag{3.42}$$

$$\dot{S}/S=[\dot{S}_0+(1/k)\dot{S}_{-1}+\cdots]/[(1/k)S_{-1}+(1/k)^2S_{-2}+\cdots]\equiv kM+M_0+(1/k)M_{-1}+\cdots, \tag{3.43}$$

implying that

$$(\dot{U}_0-L_1U_{-1})+(1/k)[\dot{U}_{-1}-(L_1U_{-2}+L_0U_{-1})]$$

$$+(1/k)^2[\dot{U}_{-2}-(L_1U_{-3}+L_0U_{-2}+L_{-1}U_{-1})]+\cdots\equiv 0, \tag{3.44}$$

$$(\dot{S}_0-M_1S_{-1})+(1/k)[\dot{S}_{-1}-(M_1S_{-2}+M_0S_{-1})]$$

$$+(1/k)^2[\dot{S}_{-2}-(M_1S_{-3}+M_0S_{-2}+M_{-1}S_{-1})]+\cdots\equiv 0. \tag{3.45}$$

The L_k and M_k are determined experimentally as functions of p. They are defined in terms of the U's and S's by putting every coefficient of $(1/k)^n$ in (3.44) and (3.45) equal to zero. Now since U_0 and U_{-1} are independent of (p^2), L_1 is independent of (p^2). The $(1/k)$ term in (3.44) shows that

[8] It is evident from the system of Eqs. (3.30) to (3.35) that $U_{-ii}=S_{-ii}$ for all values of z.

L_0 may be linear in (p^2); generally the L_{-k} is a polynomial of degree $(k+1)$ in (p^2). The same is evidently true for the M_{-k}. The coefficients of $(1/k)^n$ in (3.44) and (3.45), when put equal to zero, stand therefore for $(n+1)$ equations corresponding to the required vanishing of the individual coefficients of the powers of (p^2).

It is now possible to determine α, β and γ as functions of z from the system of equations consisting of (3.44) and (3.45), and the groups of equations starting with (3.37) and (3.30), respectively, the latter taken for $z=0$. The procedure is indicated in Table I where we have written on the left side

TABLE I. *List of unknowns and groups of equations from which they can be determined.*

U_{-10}, S_{-10}, $\dot{U}_0$, γ	(3.30), (3.38), (k^0) terms in (3.44) and (3.45)
U_{-20}, U_{-21}, S_{-20}, S_{-21}, $\dot{U}_{-10}$, $\dot{U}_{-11}$, $\dot{S}_{-10}$, $\dot{U}_0$, $\dot{\gamma}$, β	$(\dot{3.30})$, (3.31), $(3.32)_{0,\,1}$, $(3.39)_{0,\,1}$, $(1/k)$ terms in $(3.44)_{0,\,1}$, $(3.45)_{0,\,1}$
U_{-30}, U_{-31}, U_{-32}, S_{-30}, S_{-31}, S_{-32}, $\dot{U}_{-20}$, $\dot{U}_{-21}$, $\dot{U}_{-22}$, $\dot{S}_{-20}$, $\dot{S}_{-21}$, $\ddot{U}_{-10}$, $\ddot{U}_{-11}$, $\ddot{S}_{-10}$, $\ddot{U}_0$, $\ddot{\gamma}$, $\dot{\beta}$, α	$(\ddot{3.30})$, $(\dot{3.31})$, $(\dot{3.32})_{0,\,1}$, $(3.33)_{0,\,1}$, $(3.34)_{0,\,1,\,2}$, $(3.40)_{0,\,1,\,2}$ $(1/k)^2$ terms in $(3.44)_{0,\,1,\,2}$ and $(3.45)_{0,\,1,\,2}$

groups of unknowns and on the right side the corresponding groups of equations from which they can be determined. Since the set of equations starting with $(\dot{3.30})$ holds for all values of z, we can differentiate them and take the resulting equations for $z=0$. Such equations are signified by dots over the numbers of the equations. One thus finds, for example, that

$$\gamma=-1-L_1,\quad \beta=(1/2L_1)[L_0(L_1+1)+M_0(L_1-1)^2],\quad \dot{\gamma}=(\tfrac{1}{2})[L_0(L_1-1)-M_0(L_1-1)^2],\quad \text{etc.}$$

As in the case of non-dilatational disturbance one meets here with the circumstance that certain relations exist between observable quantities. Thus we must have $L_1-1=L_1/M_1$;[9] also the number of the next group of equations which determines $\ddot{\gamma}$, $\ddot{\beta}$ and $\dot{\alpha}$ exceeds the number of unknowns by one. This phenomenon is, again, an intrinsic characteristic of the differential equations and will lead to identities in an actual case.

The above theory can easily be extended to the case where simultaneously with the normal stress (p_{zz}) $P(r,t)$ there is applied a radially symmetrical radial stress $(p_{zr})-Q(r,t)$. Instead of Eq. (3.15) we shall then have, by (3.14),

$$-\mu_0\int_{-\infty}^{\infty}e^{ipt}dp\int_0^{\infty}N(p,k)kJ_1(kr)(2\dot{f}+\varphi)_0dk=Q(r,t), \tag{3.46}$$

which when inverted, yields the relation

$$N(p,k)(2\dot{f}+\varphi)_0=-(1/2\pi\mu_0)\int_0^{\infty}J_1(kr)rdr\int_{-\infty}^{\infty}Q(r,t)e^{-ipt}dt. \tag{3.47}$$

Eq. (3.47) in conjunction with (3.16), (3.17) and (3.18) determines uniquely $(\dot{f}/f)_0$, $(\dot{\psi}/\psi)_0$ and $(\psi/f)_0$, as functions of k and p. These in turn determine $(\dot{U}/U)_0$, $(\dot{S}/S)_0$ and $(S/U)_0$. Since U_0 and S_0 need not be zero now we shall have, in general,

$$\dot{U}/U=M_0+(1/k)M_{-1}+\cdots,\quad \dot{S}/S=N_0+(1/k)N_{-1}+\cdots,\quad S/U=1+(1/k)A_{-1}+\cdots, \tag{3.48}$$

the M's, N's and A's being defined by putting the coefficients of the powers of $(1/k)$ in

[9] The relation $\gamma=-1-L_1$ is of the same type, since $\gamma=(\lambda/\mu)_0$ can be determined independently.

$$(\dot{U}_0 - U_0M_0) + (1/k)[\dot{U}_{-1} - (U_0M_{-1} + U_{-1}M_0)]$$

$$+ (1/k)^2[\dot{U}_{-2} - (U_0M_{-2} + U_{-1}M_{-1} + U_{-2}M_0)] + \cdots, \quad (3.49)$$

$$(\dot{S}_0 - S_0N_0) + (1/k)[\dot{S}_{-1} - (S_0N_{-1} + S_{-1}N_0)] + (1/k)^2[\dot{S}_{-2} - (S_0N_{-2} + S_{-1}N_{-1} + S_{-2}N_0)] + \cdots, \quad (3.50)$$

and in

$$(1/k)[S_{-1} - (U_{-1} + U_0A_{-1})] + (1/k)^2[S_{-2} - (U_{-2} + U_{-1}A_{-1} + U_0A_{-2})] + \cdots, \quad (3.51)$$

equal to zero. Eq. (3.41) will still be true, but $U_{-ii}(=S_{-ii})$ need not be zero at the surface.

With the M's, N's and A's known as functions of (p^2), the determination of λ, μ and ρ can be carried out as in the previous section, with the only difference that Eqs. (3.49) and (3.50) now take the place of (3.44) and (3.45), while Eq. (3.51) replaces the system of equations starting with (3.37). One thus finds

$$\beta = (\tfrac{1}{2})[(\gamma+1)A_{-10} - (\gamma+3)M_0],$$

$$\dot{\beta} = (\gamma+1)A_{-20} - \beta(A_{-10} + \beta + M_0) + (\gamma+2)A_{-10}M_0 - M_{-10} - (\gamma+2)N_{-10}, \quad \alpha = -(\gamma+1)A_{-21} + (\gamma+3)M_{-11}$$

$$\dot{\gamma} = [2(\gamma+2)(N_{-10} - M_{-10} + M_0A_{-10}) + (\gamma+1)(\dot{\beta} + \beta M_0)$$

$$+ (\tfrac{1}{2})(\gamma+3)(\gamma+1)\beta(A_{-10} - M_0)]/(M_0 - A_{-10}), \text{ etc.}$$

It follows that when the (radially symmetrical) normal and radial stresses applied at the surface are known, it is possible to determine from the observed surface motion the variation with depth of ρ, μ and λ.

4. Conclusions

We can sum up our results as follows: The motion of a heterogeneous half-space resolves itself, as in a homogeneous medium, into two types: one—unaccompanied by dilatation, and one which is accompanied by dilatation. If the motion is to have cylindrical symmetry, the stresses applied at the surface must also have cylindrical symmetry and, furthermore, in the case of a non-dilatational disturbance the only possible stress is the azimuthal ($p_{z\theta}$), while in the case of a dilatational disturbance, the possible stresses are the normal (p_{zz}) and the radial (p_{zr}). In the former case the motion is horizontal and in the azimuthal direction (v), in the second case the motion takes place in planes through the vertical, the azimuthal displacement being zero. If normal, radial and azimuthal stresses, of known space and time distributions, are applied simultaneously at the surface and the subsequent surface motion is observed, one can determine $\rho(z)$ and $\mu(z)$ from v alone and $\rho(z)$, $\mu(z)$ and $\lambda(z)$ from u and w alone.

It is a pleasure to acknowledge my indebtedness to Professor L. B. Slichter who suggested the problem and directed the research. I also wish to express my appreciation to Professor R. E. Langer for having criticised the paper in manuscript.

Study of Emergence Angle and Propagation Paths of Seismic Waves

MAURICE EWING AND A. P. CRARY, *Lehigh University*

(Received May 24, 1934)

Travel-time curves are given for elastic waves through the earth in a region in which the velocity increases continuously with depth. These time-distance curves have been approximated by an equation of the form $X=aT^2+bT$ from which the velocity depth relation has been deduced. A new method for measurement of the emergence angle has been used and the values obtained agree reasonably well with those deduced from theoretical treatment of the time-distance curve. Formulas for the travel-time between any two points in the medium under consideration are derived. These formulas agree closely with two sets of direct measurements. In one of these the seismograph was placed at various distances directly beneath the explosion. In the second case it was placed at a fixed depth beneath the surface and the explosion was located on the surface at various distances. The approximate depth to bed rock is obtained from the time-distance curves by use of the formulas mentioned above.

THE theory of the propagation of elastic waves through the earth in a region in which the velocity increases with depth in such a fashion that the observed time-distance curve may be represented by the equation

$$X=aT^2+bT \tag{1}$$

has been treated by Ewing and Leet.[1] The present paper includes an extension of the theory and an experimental investigation of many points in connection therewith. The data used were taken near Green Pond, Northampton County, Pennsylvania. The material at the surface was a fine grained alluvial deposit, which was underlain by limestone. The surface of the limestone was probably quite irregular.

TIME-DISTANCE DATA AND VELOCITY-DEPTH DETERMINATION

The time-distance data are shown in Fig. 1. The curved lines drawn represent Eq. (1) with

$$a=29{,}690 \text{ ft./sec.}^2, \quad b=752.9 \text{ ft./sec.}$$

The values of these constants were obtained by a least square solution which included all points representing wave paths lying entirely in the upper layer. By use of the following equations

$$V=2\,aT+b, \tag{2}$$

$$b/\sin\theta_0=v/\sin\theta=V, \tag{3}$$

$$P=b^2/8\pi a(\sinh q-q),^1 \tag{4}$$

$$q=2 \text{ arc cosh } V/b$$

the velocity depth relation is determined. Here V is the velocity at the midpoint of the path of length X and maximum penetration P, and θ_0 is the emergence angle for this path. Fig. 2 illustrates the meaning of each of these symbols. The

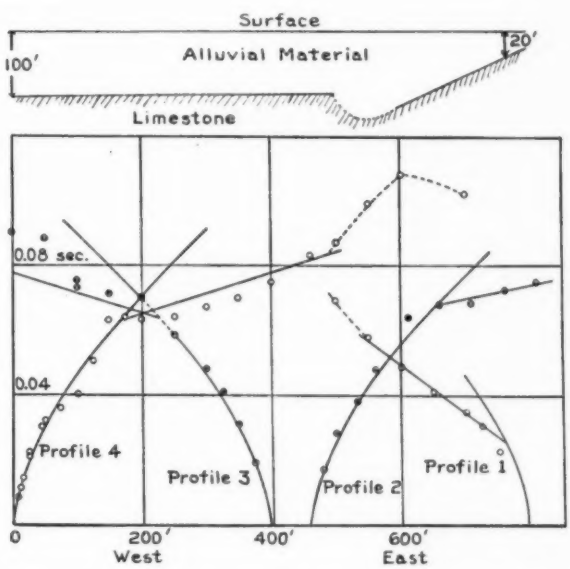

FIG. 1. Time-distance curves and approximate section at Green Pond.

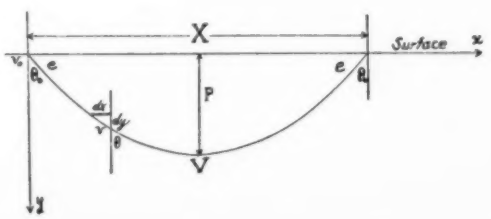

FIG. 2. Diagram of wave path.

[1] Ewing and Leet, Trans. A.I.M.E. Geophysical Prospecting (1932).

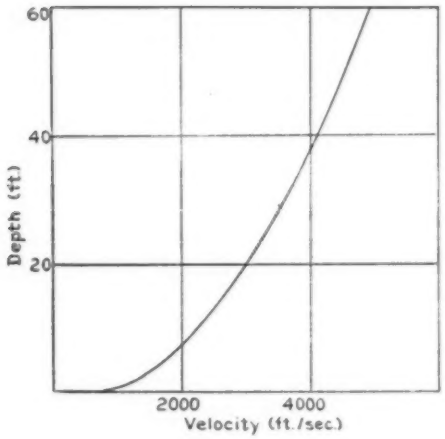

FIG. 3. Velocity-depth relation (Green Pond).

velocity-depth curve thus obtained is shown in Fig. 3.

EMERGENCE ANGLE

A new method was used to measure the emergence angle θ_0 of the waves. The seismograph was of the type technically known as a geophone. It was originally designed to measure only vertical motions but after an alteration of the spring suspension was made it would operate when tilted at any angle between the vertical

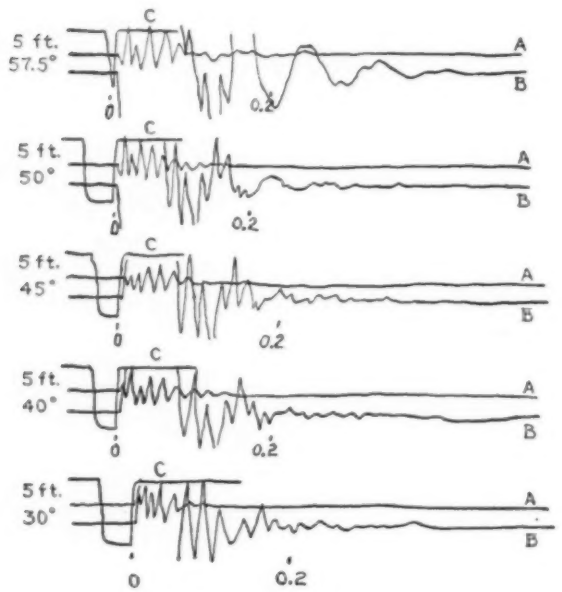

FIG. 4. Seismograms illustrating method used to determine emergence angle. Angles given represent tilt of seismograph from vertical position. A, low sensitivity; B, high sensitivity; C, timing line.

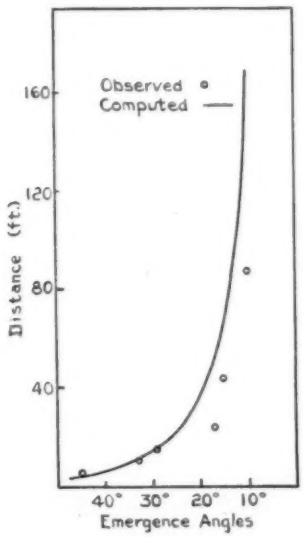

FIG. 5. Relation of emergence angle to distance traversed.

and the horizontal. The tilting produced some change in the constants of the instrument, but this change was of no importance in the investigation. The idea of the experiment was to tilt the geophone toward the shot until its axis became perpendicular to the direction of the first motion produced by the shot. Successive tests were made to determine the angle of tilt at which the direction of first motion on the seismogram showed a reversal. (This angle could easily be determined to one or two degrees in the range of distances studied.) Fig. 4 shows the set of observations taken at 5 feet. In Fig. 5 emergence angle θ_0 is plotted against the distance traversed by the wave along the surface. The curve drawn represents the theoretical values of the angle as determined from Eq. (3) using the values of a and b obtained from the time-distance curves. The observed values, indicated by the points, agree with the calculated values within the limits of experimental error. It was not considered necessary to correct for the difference between true and apparent emergence angles.[2]

TRAVEL-TIME BETWEEN ANY TWO POINTS ON A PATH

From Eq. (4) the relation

$$dy/dv = (v^2 - b^2)^{\frac{1}{2}}/2\pi a, \tag{5}$$

[2] E. Wiechert, Gott. Nachr. 1907, No. I.

where v is the velocity at the depth y, is obtained. Eq. (2) yields

$$dy/dx = \pm(b^2 \csc^2 \theta_0 - v^2)^{\frac{1}{2}}/v, \qquad (6)$$

which may be combined with (5) to give the relation:

$$x = \pm(1/2\pi a)\int_b^v v[(v^2-b^2)/(b^2 \csc^2 \theta_0 - v^2)]^{\frac{1}{2}}dv$$

$$= (b^2 \cot^2 \theta_0/4\pi a)[\alpha - \sin \alpha \cos \alpha], \qquad (7)$$

where $\sin \alpha = \pm \tan \theta_0(v^2/b^2-1)^{\frac{1}{2}}$. The positive sign should be taken if the wave has not reached its maximum depth.

The travel-time $t = \int ds/v$ becomes, upon substitution from (5) and (6)

$$t = \pm(b/2\pi a \sin \theta_0)\int_b^v (1/v)$$

$$\times[(v^2-b^2)/(b^2 \csc^2 \theta_0 - v^2)]^{\frac{1}{2}}dv$$

$$= (b/2\pi a \sin \theta_0)$$

$$\times[\alpha - \sin \theta_0 \tan^{-1}(\tan \alpha/\sin \theta_0)]. \qquad (8)$$

For the limiting case, $\theta_0 = 0$, the path is vertical and (7) and (8) become

$$x = 0 \qquad (7')$$

$$t = (b/2\pi a)[(v^2/b^2-1)^{\frac{1}{2}} - \tan^{-1}(v^2/b^2-1)^{\frac{1}{2}}]. \qquad (8')$$

Formulas (7) and (8) make it possible to calculate the time required to traverse any part of any path. Two sets of data were taken to which these formulae may be applied. In the first case records were taken with the geophone buried at a series of depths up to about 20 ft., the shot in each case being at the surface directly above. In the second case the geophone remained at a depth of 18.5 ft. while shots were fired on the surface at various distances from the mouth of the hole. Figs. 6 and 7 compare the travel-time obtained from these observations with those computed from the above equations using the values of a and b as computed from the time-distance curves.

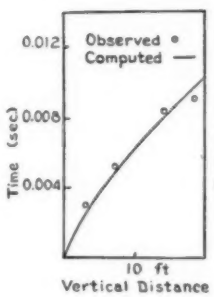

FIG. 6.

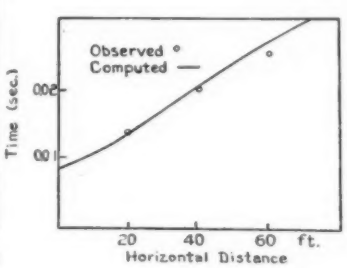

FIG. 7.

FIG. 6. Travel time curve for waves travelling vertically.
FIG. 7. Travel time curve for waves travelling from surface to depth of 18′ 6″.

WAVES REFLECTED OR REFRACTED AT DISCONTINUITIES

By use of the formulas developed in the preceding section it is possible to calculate time-distance curves for waves reflected or refracted at the surface of a layer of rocks covered by material in which the velocity increases with depth in the manner discussed above. For a given depth the velocity v is given by Eq. (4). From Eqs. (7) and (8) it is possible to calculate time-distance curves for waves reflected at this depth by assuming a series of values for θ_0. If the reflecting surface is horizontal the time and the distance will be just double that calculated from these equations. If the reflecting surface is sloping it is necessary to make separate calculations for the incident and the reflected waves.

In the case of waves which are refracted along the surface of a buried rock the angle of emergence is known from the velocity of the refracting layer. If, then, a depth is assumed the horizontal distance and the time of the wave in the upper layer can be computed from the value of the emergence angle and the velocity in the upper layer corresponding to the depth assumed, as in the case of reflected waves. The remainder of the distance traversed is in the higher speed material and the total time is the sum of the time spent there and the time of the incident and emergent rays in the upper layer.[3] For waves refracted along a sloping layer, the computations become increasingly more difficult as the emergence angle depends not only on the velocity of the high speed layer but also upon its depth.

Although the primary purpose of the present work was to study waves propagated in the upper layer, the data represented in Fig. 1 afford a good illustration of refracted waves. The

[3] Rutherford, Am. Geophys. Union. Trans., p. 292, 1933.

straight lines drawn in Profiles 3 and 4 represent an assumed horizontal layer which is 100 ft. beneath the surface and has a velocity of 17,000 ft./sec. Because of irregularities in the surface of the rock the observed points deviate considerably from the lines, but the depth assumed is certainly accurate to 5 or 10 percent. Profiles 1 and 2 indicate a limestone surface sloping up sharply to the east. By the aid of Fig. 6 the depth at the east end may be estimated at approximately 20 ft. In the region between the 500 and 600 ft. stations there are systematic deviations marked by dotted lines on the time-distance curve. These indicate a fairly sharp depression in the surface of the limestone between these stations. The deviations of the points in general are an indication of the roughness of the limestone surface. An approximate cross section of this region is shown in Fig. 1.

Professor B. L. Miller of the Department of Geology, of Lehigh University, who recommended the location which was chosen for these experiments, has suggested that the structure of the limestone revealed by these results represents the buried valley of a pre-glacial stream.

We are indebted to the Geophysical Research Corporation for the seismic instruments, to the Trojan Powder Company for the explosives, to Mr. H. S. Snyder upon whose property the experiments were carried out, and to Mr. A. M. Thorne, Jr., for assistance with the experimental observations.

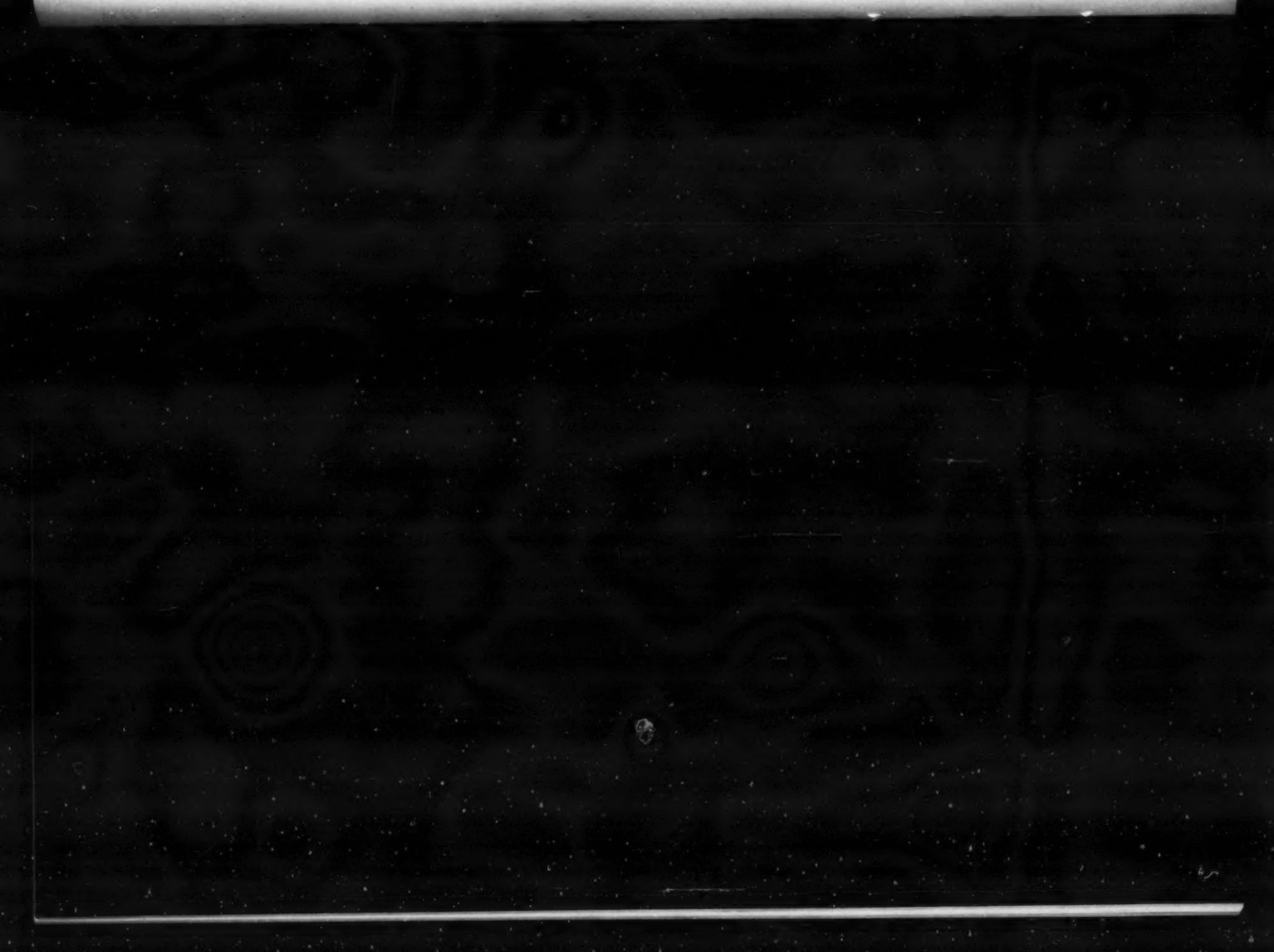

Notice to Contributors

Manuscripts

Send manuscripts to John T. Tate, University of Minnesota, Minneapolis, Minnesota.

Papers must be in English, typewritten double spaced with wide margins.

Abstracts

An abstract must accompany each article. It should be adequate as an *index* and as a *summary*. As an index it should give all subjects, major and minor, concerning which new information is presented. As a summary it should give the conclusions of the article and all numerical results of general interest.

References

References should appear as foot notes, numbered consecutively, and arranged thus:

A. B. Smith, Phys. Rev. **41**, 852 (1932).

Captions and Legends

Legends for figures must accompany manuscript. Each table should have a caption. These in all cases should be complete in themselves so as to make the data intelligible to the reader without reference to the text.

Mathematical Expressions

Make all expressions clear to the typesetter. Identify in the margin of the manuscript Greek letters and unusual symbols.

Use fractional exponents instead of root signs.

Avoid complicated exponents and subscripts. Should it be necessary to repeat a complicated expression a number of times it should be represented by some convenient symbol.

The solidus (/) should be used wherever possible for fractions.

Illustrations

Plan figures for approximately one-half reduction. Wherever possible arrange figures so that after reduction they will not be wider than three inches. Lettering must be large enough to be readable after reduction.

Line drawings must be made with India ink on white paper or tracing cloth. Coordinate paper is not desirable, but if used must be blue-lined and all coordinates to be reproduced drawn with India ink.

Drawings which cannot be used will be returned to the author or redrawn at his expense.

Photographs should show clear black and white contrasts.

Avoid round and oval photographs.

Publication Charge

A portion of the cost of publishing the results of research must be regarded as an integral part of the cost of the research. In keeping with the policy which is effective for the Institute's publications a bill for $3.00 per page will be sent to the authors of papers appearing in this journal. It is intended that the authors shall present these bills for payment to the institutions which have supported their researches. If the institution is unable to make payment the bills are to be returned marked "No Funds Available."

Reprints

As a partial return for the publication charge one hundred reprints without covers will be furnished free. Additional reprints may be obtained at a regular schedule of prices.

Alterations

Take great care that each manuscript is typographically accurate. A limited number of alterations in proof are unavoidable, but the cost of making extensive alterations after the article has been set in type will be charged to the author.

Proof and all correspondence concerning papers in the process of publication should be addressed to the Editorial Secretary, American Institute of Physics, 11 East 38th Street, New York, N. Y.

THE AMERICAN PHYSICAL SOCIETY

ARTHUR H. COMPTON, *President*
University of Chicago
Chicago, Illinois

R. W. WOOD, *Vice-President*
The Johns Hopkins University
Baltimore, Maryland

W. L. SEVERINGHAUS, *Secretary*
Columbia University
New York, New York

G. B. PEGRAM, *Treasurer*
Columbia University
New York, New York

JOHN T. TATE, *Editor*
University of Minnesota
Minneapolis, Minnesota

L. B. LOEB, *Local Secretary for the Pacific Coast*
University of California
Berkeley, California

THE object of the American Physical Society is the advancement and diffusion of the knowledge of physics. It sponsors *The Physical Review*, *Physics* and the *Reviews of Modern Physics*. Upon the recommendation of two or more members, any person engaged in work in the field of physics or actively interested in physics may become a member; receive one of the journals; receive also *Science Abstracts* A, *The Review of Scientific Instruments with Physics News and Views*, and the Bulletin of all meetings; and attend and participate in the seven annual meetings.

Annual dues: $10. Fellows, $14.

For further information address the Secretary as above.

THE SOCIETY OF RHEOLOGY

S. E. SHEPPARD, *President*
Eastman Kodak Company
Rochester, New York

EUGENE C. BINGHAM, *Editor*
Lafayette College
Easton, Pennsylvania

A. STUART HUNTER, *Secretary & Treasurer*
Du Pont Rayon Company
Buffalo, New York

THE Society of Rheology was formed in 1929 to advance the science of the deformation and flow of matter. It cooperates with the American Physical Society in editing *Physics* of which four issues per year are devoted to *Rheology*. All persons interested are invited to become members and participate in the proceedings at the annual December meetings. Members receive without other charge than their dues all issues of *Physics*, *The Review of Scientific Instruments with Physics News and Views* and the notices of the Society.

Annual dues: $6.

For further information address the Secretary as above.